

---

# Estimating Conditional Mutual Information for Dynamic Feature Selection

---

**Soham Gadgil\***  
University of Washington  
sgadgil@uw.edu

**Ian Covert\***  
University of Washington  
icovert@uw.edu

**Su-In Lee**  
University of Washington  
suinlee@uw.edu

## Abstract

Dynamic feature selection, where we sequentially query features to make accurate predictions with a minimal budget, is a promising paradigm to reduce feature acquisition costs and provide transparency into the prediction process. The problem is challenging, however, as it requires both making predictions with arbitrary feature sets and learning a policy to identify the most valuable selections. Here, we take an information-theoretic perspective and prioritize features based on their mutual information with the response variable. The main challenge is learning this selection policy, and we design a straightforward new modeling approach that estimates the mutual information in a discriminative rather than generative fashion. Building on our learning approach, we introduce several further improvements: allowing variable feature budgets across samples, enabling non-uniform costs between features, incorporating prior information, and exploring modern architectures to handle partial input information. We find that our method provides consistent gains over recent state-of-the-art methods across a variety of datasets.

## 1 Introduction

Many machine learning applications rely on high-dimensional datasets with significant data acquisition costs. For example, medical diagnosis can depend on a range of demographic features, lab tests and physical examinations, and each piece of information takes time and money to obtain [24, 35, 40]. To improve interpretability and reduce data acquisition costs, a natural approach is to adaptively query features given the current information, so that each prediction relies on only a small number of features. This approach is referred to as *dynamic feature selection* (DFS),<sup>1</sup> and it is a promising paradigm that has been considered by several works in recent years [14, 15, 18, 39, 40].

Among the existing methods that address this problem, two main approaches have emerged. One idea is to formulate DFS as a Markov decision process (MDP) and use reinforcement learning (RL) [22, 39, 40, 52]. This approach has the capacity to discover the optimal policy, but it faces training difficulties that are common in RL [36]. Alternatively, another line of work focuses on greedy approaches, where features are selected based on their conditional mutual information (CMI) with the response variable [16, 49]. While less flexible, the greedy approach is near-optimal under certain assumptions about the data distribution [16] and has been found to work well in practice [15, 18].

Nevertheless, the greedy approach is non-trivial to implement because calculating the CMI requires detailed knowledge of the data distribution (see Section 2.2). Many recent works have explored approximating the CMI using generative models [14, 35, 49, 57], but these methods face a challenging modeling problem [50, 54, 57] and lead to a slow CMI estimation process [35]. Instead, two recent

---

\*Equal contribution.

<sup>1</sup>The problem has also been referred to as *sequential information maximization* [16] *active variable selection* [49] and *information pursuit* [15].

works introduced a simpler approach, which is to directly estimate the feature index with maximum CMI [15, 18]. These methods rely on simpler learning objectives, are faster at inference time, and often provide better predictive accuracy. They can be thought of *discriminative* alternatives to earlier generative methods [55], and their main downside is that they bypass estimating the CMI, which can be useful for multiple purposes (e.g., determining when to stop selecting new features).

Here, our goal is to advance the greedy DFS approach by combining the best aspects of current methods: building on recent work [15, 18], we aim to estimate the CMI itself in a discriminative fashion. We aim to do so without requiring additional labels, making strong assumptions about the data distribution, or fitting generative models. We find that this is possible by designing a suitable learning objective, which we prove recovers the CMI if our model is trained to optimality (Section 4). Based on this, we then explore a range of capabilities enabled by accurately estimating the CMI: these include accounting for non-uniform feature costs, trading off feature cost and information in multiple ways, and leveraging modern architectures to improve our learning approach.

We find that our proposal offers a promising alternative to available methods: it enables the advantages of generative methods while retaining the simplicity of discriminative methods, and it shows improved performance in our experiments. The contributions of this work are the following:

1. We develop a learning approach to estimate the CMI in a discriminative fashion. Our method involves training a network to score candidate features based on their predictive utility, and we prove that training with our objective recovers the exact CMI at optimality.
2. We generalize our approach to incorporate prior information beyond the main features. Here, we again prove that our procedure recovers a modified version of the CMI at optimality.
3. Taking inspiration from adaptive submodular optimization, we show how to adapt our CMI-based approach to scenarios with non-uniform feature costs.
4. We analyze the role of variable feature budgets and how they enable an improved cost-accuracy tradeoff. We show that a single instantiation of our method can be evaluated with multiple stopping criteria, and that a policy with no per-prediction budget constraints should perform best.
5. We investigate the role of modern architectures in improving performance in DFS. In particular, we find that for image data, our method benefits from using ViTs rather than standard CNNs.

Our experiments demonstrate the effectiveness of our approach across a range of applications, including several tabular and image datasets. We compare our approach to many recent methods, and we find that our approach provides consistent gains across all the datasets we tested.

## 2 Problem formulation

Here, we introduce notation used throughout the paper and describe our problem formulation.

### 2.1 Notation

Let  $\mathbf{x}$  denote a vector of input features and  $\mathbf{y}$  a response variable for a supervised learning task. The input consists of  $d$  separate features  $\mathbf{x} = (\mathbf{x}_1, \dots, \mathbf{x}_d)$ , and we use  $S \subseteq [d] \equiv \{1, \dots, d\}$  to denote a subset of indices and  $\mathbf{x}_S = \{\mathbf{x}_i : i \in S\}$  a subset of features. Bold symbols  $\mathbf{x}, \mathbf{y}$  represent random variables, the symbols  $x, y$  are possible values, and  $p(\mathbf{x}, \mathbf{y})$  denotes the data distribution.

Our goal is to select features given the currently available information, and do so on a per-instance basis to rapidly arrive at accurate predictions. In doing so, we require a predictor  $f(\mathbf{x}_S)$  that makes predictions given any set of available features; for example, if  $\mathbf{y}$  is discrete then its predictions lie in the simplex, or  $f(\mathbf{x}_S) \in \Delta^{K-1}$  for  $K$  classes. We also require a selection policy  $\pi(\mathbf{x}_S) \in [d]$ , which takes a set of features as its input and outputs the next feature index to observe. We next discuss how to design these models, focusing on an approach motivated by information theory.

### 2.2 Dynamic feature selection

The goal of DFS is to select features separately for each prediction, and achieve both low acquisition cost and high predictive accuracy. Previous work has explored several approaches to design a selection policy, including training the policy with RL [39, 40], imitation learning [32, 33], and

following a greedy policy based on CMI [15, 18, 49, 57]. We focus here on the latter approach, where the idealized policy selects the feature with maximum CMI at each step, or where we define  $\pi^*(x_S) = \arg \max_i I(\mathbf{y}; \mathbf{x}_i | x_S)$ . Note that the CMI is equal to the following KL divergence [17]:

$$I(\mathbf{y}; \mathbf{x}_i | x_S) = D_{\text{KL}}(p(\mathbf{x}_i, \mathbf{y} | x_S) || p(\mathbf{x}_i | x_S)p(\mathbf{y} | x_S)). \quad (1)$$

This approach therefore identifies the most informative feature at each step; which is consistent with performing greedy uncertainty minimization [18], and the same idea is also the basis of Bayesian experimental design [9, 48]. The idealized selection policy is accompanied by an idealized predictor, which is the Bayes classifier  $f^*(x_S) = p(\mathbf{y} | x_S)$  for classification problems.

It is known that under certain assumptions about the data distribution, greedily selecting features with  $\pi^*(x_S)$  provides performance within a multiplicative factor of the optimal policy [16]. However, the CMI policy is difficult to implement because it requires oracle access to the data distribution: computing eq. (1) requires both the response and feature distributions  $p(\mathbf{y} | x_S)$  and  $p(\mathbf{x}_i | x_S)$  for all  $(S, i)$ , which presents a challenging modeling problem. Some works have approximated  $I(\mathbf{y}; \mathbf{x}_i | x_S)$  using generative models [14, 35, 49, 57], while others have directly modeled  $\pi^*(x_S)$  [15, 18].

When we follow the greedy CMI policy, another question that remains is how many features to select for each prediction. Previous work has focused mainly on the fixed-budget setting [15, 16, 18, 49, 57], where we stop given  $x_S$  when  $|S| = k$  for a specified budget  $k < d$ . We instead consider variable budgets in this work, where the goal is to achieve high accuracy given a low *average feature cost*. Unlike many works, we also consider non-uniform costs for each feature. As we discuss in Section 4, these goals are made easier by our method for estimating the CMI in a discriminative fashion.

### 3 Related work

One of the earliest works on DFS is Geman and Jedynak [28], who used CMI as a selection criterion but made simplifying assumptions about the data distribution. Chen et al. [16] analyzed the greedy CMI approach from a theoretical perspective and showed conditions under which it achieves near-optimal performance. More recent works have focused on practical implementations: among them, several focused on generative modeling approaches to approximate the CMI [14, 35, 49, 57], and two concurrent works proposed discriminative approaches that directly predict the optimal feature index [15, 18]. Our work develops a similar discriminative approach, but in order to estimate the CMI itself rather than the argmax, which bypasses the need for complex generative models

Apart from these, many works have addressed DFS as an RL problem [22, 39, 40, 46, 60]. For example, Janisch et al. [39] formulate DFS as a MDP where the reward is the 0-1 loss minus the feature cost. RL theoretically has the capacity to discover better policies than a greedy approach, but it has not been found to perform well in practice [15, 18, 24], seemingly due to training difficulties that are common in RL [36]. Other works have instead explored the use of imitation learning, where selections are made by mimicking an oracle policy [32, 33].

Finally, static feature selection has been an important subject in statistics and machine learning for decades; see [11, 31, 45] for reviews. CMI is also at the basis of some static methods, see Fleuret [27] for example. Greedy methods have been proven to perform well under certain assumptions about the data distribution [19, 23], and such methods are popular for models that are inexpensive to fit (e.g., linear regression). Feature selection with neural networks is more challenging, but methods now exist that leverage either group sparse penalties [26, 44, 62] or differentiable gating mechanisms [7, 13, 47]. Such gating approaches were the basis for recent DFS methods [15, 18], but our work bypasses these techniques with a simpler regression objective.

## 4 Proposed method

In this section, we introduce our method to dynamically select features by estimating the CMI in a discriminative fashion. We then discuss how to incorporate prior information into the selection process, handle non-uniform feature costs, and enable variable budgets across predictions.

### 4.1 Estimating the conditional mutual information

We parameterize two networks to implement our selection policy. First, we have a predictor network  $f(\mathbf{x}_S; \theta)$ , e.g., a classifier with predictions in  $\Delta^{K-1}$ . Next, we have a value network  $v(\mathbf{x}_S; \phi) \in \mathbb{R}^d$

designed to estimate the CMI for each feature, or  $v_i(x_S; \phi) \approx I(\mathbf{y}; \mathbf{x}_i | x_S)$ . These are implemented with zero-masking to indicate missing features, and we can also pass the mask as a binary vector to indicate missing values. Once they are trained, we make selections according to  $\arg \max_i v_i(\mathbf{x}_S; \phi)$ , and we can make predictions at any time using  $f(\mathbf{x}_S; \theta)$ . The critical question is how to train the networks effectively, given that prior work required generative models to estimate the CMI [14, 49].

Our main insight is to train the models jointly but with their own objectives, and to design an objective for the value network that recovers the CMI at optimality. Specifically, we formulate a regression problem whose target is the incremental improvement in the loss when incorporating a single new feature. We train the predictor to make accurate predictions given any feature set, or

$$\min_{\theta} \mathbb{E}_{\mathbf{x}_Y} \mathbb{E}_S [\ell(f(\mathbf{x}_S; \theta), y)], \quad (2)$$

and we simultaneously train the value network with the following regression objective,

$$\min_{\phi} \mathbb{E}_{\mathbf{x}_Y} \mathbb{E}_S \mathbb{E}_i \left[ (v_i(\mathbf{x}_S; \phi) - \Delta(\mathbf{x}_S, \mathbf{x}_i, \mathbf{y}))^2 \right], \quad (3)$$

where we define the loss improvement as  $\Delta(x_S, x_i, y) = \ell(f(x_S; \theta), y) - \ell(f(x_{S \cup i}; \theta), y)$ . The regression objective in eq. (3) is motivated by the following property, which shows that if we assume an accurate predictor  $f(\mathbf{x}_S; \theta)$  (i.e., the Bayes classifier), the value network’s labels are unbiased estimates of the CMI (proofs are in Appendix A).

**Lemma 1.** *When we use the Bayes classifier  $p(\mathbf{y} | \mathbf{x}_S)$  as a predictor and  $\ell$  is cross entropy loss, the incremental loss improvement is an unbiased estimator of the CMI for each  $(x_S, \mathbf{x}_i)$  pair:*

$$\mathbb{E}_{\mathbf{y}, \mathbf{x}_i | x_S} [\Delta(x_S, \mathbf{x}_i, \mathbf{y})] = I(\mathbf{y}; \mathbf{x}_i | x_S). \quad (4)$$

Based on this result and the fact that the optimal predictor does not depend on the selection policy [18], we can make the following claim about jointly training the two models. We assume that both models are infinitely expressive (e.g., very wide networks) so that they can achieve their respective optimizers.

**Theorem 1.** *When  $\ell$  is cross entropy loss, the objectives eq. (2) and eq. (3) are jointly optimized by a predictor  $f(x_S; \theta^*) = p(\mathbf{y} | x_S)$  and value network where  $v_i(x_S; \phi^*) = I(\mathbf{y}; \mathbf{x}_i | x_S)$  for  $i \in [d]$ .*

This allows us to train the models in an end-to-end fashion using stochastic gradient descent, see Figure 1. In Appendix A we prove a similar result for regression problems: that the policy estimates the reduction in conditional variance associated with each candidate feature. Additional analysis in Appendix B shows how suboptimality in the classifier can affect the learned CMI estimates; however, even if the learned estimates  $v_i(\mathbf{x}_S; \phi)$  are imperfect in practice, we expect good performance because the policy replicates selections that yield large loss improvements during training.

Several other steps are important during training, and these are detailed in Appendix C. First, like several prior methods, we pre-train the predictor with random feature sets before beginning joint training [15, 18, 57]. Next, we generate training samples  $(x_S, x_i, y)$  by executing the current policy with a random exploration probability  $\epsilon \in [0, 1]$ , which can be decayed throughout training. Finally, we sometimes share parameters between the models, particularly when they are large; this helps in our experiments with image data, which use either CNNs or ViTs [21].

## 4.2 Incorporating prior information

A further direction is utilizing *prior information* obtained before beginning the selection process. We view such prior information as a separate random variable  $\mathbf{z}$ , and it can be either an exogenous input, a subset of features that are available with no associated cost, or even a noisy or low-resolution version of the real input  $\mathbf{x}$  [5, 6, 58]. Situations of this form arise in multiple applications, e.g., a patient’s demographic features in a medical diagnosis setting.

Given such prior information, our idealized DFS policy should be modified as follows. First, the selections must be based on  $I(\mathbf{y}; \mathbf{x}_i | x_S, z)$ , which captures how informative  $\mathbf{x}_i$  is given knowledge of both  $\mathbf{x}_S$  and  $\mathbf{z}$ . Next, the predictions made at any time are given by  $p(\mathbf{y} | x_S, z)$ , because  $\mathbf{z}$  provides information that can improve our predictions. As for our proposed CMI estimation procedure in Section 4.1, it is straightforward to modify. The two models must take the prior information  $\mathbf{z}$  as an additional input, and we can train them with modified versions of eqs. (2) and (3),

$$\min_{\theta} \mathbb{E}_{\mathbf{x}_Y \mathbf{z}} \mathbb{E}_S [\ell(f(\mathbf{x}_S, \mathbf{z}; \theta), y)], \quad \min_{\phi} \mathbb{E}_{\mathbf{x}_Y \mathbf{z}} \mathbb{E}_S \mathbb{E}_i \left[ (v_i(\mathbf{x}_S, \mathbf{z}; \phi) - \Delta(\mathbf{x}_S, \mathbf{x}_i, \mathbf{z}, \mathbf{y}))^2 \right], \quad (5)$$

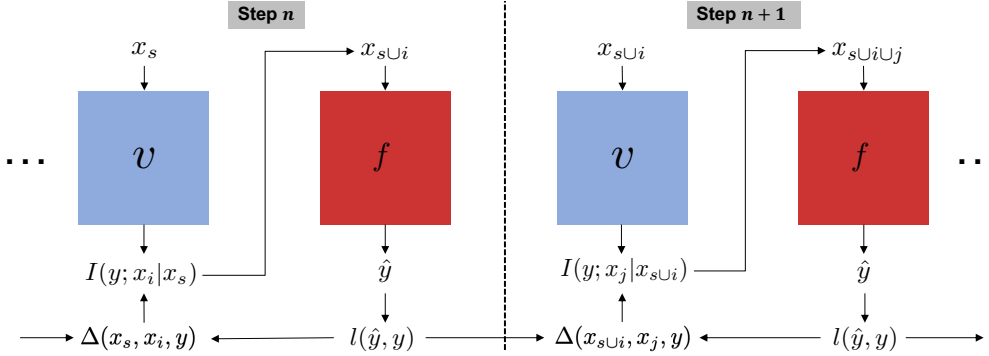


Figure 1: Diagram of our training approach. At each selection step  $n$ , the value network  $v(x_s; \phi)$  predicts the CMI for all features, and a single feature  $x_i$  is chosen for the next prediction  $f(x_{s \cup i}; \theta)$ . The prediction loss is used to update the predictor (see eq. (2)), and the loss improvement is used to update the value network (see eq. (3)). The networks are trained jointly with SGD.

where  $\Delta(x_S, x_i, z, y) = \ell(f(x_S, z; \theta), y) - \ell(f(x_{S \cup i}, z; \theta), y)$  is the incremental loss improvement. We then have the following result for jointly training the two models.

**Theorem 2.** *When  $\ell$  is cross entropy loss, the objectives in eq. (5) are jointly optimized by a predictor  $f(x_S, z; \theta^*) = p(\mathbf{y} | x_S, z)$  and value network where  $v_i(x_S, z; \phi^*) = I(\mathbf{y}; \mathbf{x}_i | x_S, z)$  for all  $i \in [d]$ .*

The same implementation details discussed in Section 4.1 apply here, and as before, we expect strong performance even if the CMI estimates  $v_i(\mathbf{x}_S, \mathbf{z}; \phi)$  do not reach their optimal values in practice.

### 4.3 Allowing a variable feature budget

Given our approach for estimating each feature’s CMI, a natural question is how to trade off information with feature acquisition costs. We now consider two challenges related to features costs: (1) how to handle non-uniform costs between features, and (2) when to stop collecting new features.

**Non-uniform costs** For the first challenge, consider medical diagnosis as a motivating example. Diagnoses can be informed by heterogeneous data, including demographic variables, questionnaires, physical examinations, and lab tests; each measurement can require a different amount of time or money [24, 40], and feature costs must be balanced with the information they provide. For simplicity, we consider that each feature has a cost  $c_i > 0$  and that costs are additive across features.

There are multiple ways to trade off cost with information, but we take inspiration from adaptive submodular optimization, where item costs are accounted for via the ratio between the expected improvement and cost. Here, this suggests that our selections should be  $\arg \max_i I(\mathbf{y}; \mathbf{x}_i | x_S) / c_i$ . For adaptive submodular objectives, this criterion guarantees near-optimal performance [30]; the DFS problem is known *not* to be adaptive submodular [16], which means that we cannot offer performance guarantees, but we find that this approach works well in practice (see Section 5).

**Variable budgets** Next, we consider when to stop acquiring new features. Many previous works focused on the budget-constrained setting, where we adopt a budget  $k$  for all predictions [16, 18, 49, 57]. This can be viewed as a stopping criterion, and it generalizes to non-uniform costs: we can keep collecting new information as long as  $\sum_{i \in S} c_i \leq k$ . Alternatively, we can adopt a confidence-constrained setup [15], where selection terminates once the predictions have low uncertainty. For classification problems, a natural approach is to stop collecting features when  $H(\mathbf{y} | x_S) \leq m$ .

In general, it is unclear whether we should adopt a budget- or confidence-constrained approach, or whether there is another option that offers a better cost-accuracy tradeoff. We resolve this question by considering the optimal performance achievable by *non-greedy policies*, and we present the following insight: that policies with per-prediction constraints are Pareto-dominated by those that achieve their constraints *on average*. The following proposition states this in a simplified form, and we defer the formal version to Appendix A due to the extra setup and notation it requires.

**Proposition 1.** (Informal) For any feature budget  $k$ , the best policy to achieve this budget on average achieves lower loss than the best policy with a per-prediction budget constraint. Similarly, for any confidence level  $m$ , the best policy to achieve this confidence on average achieves lower cost than the best policy with a per-prediction confidence constraint.

Intuitively, when designing a policy to achieve a given average cost or confidence level, it can help to let the policy violate that level for certain predictions. If we only care about the average cost or accuracy, it does not help to constrain the policy on a per-prediction level. For example, for a patient whose medical condition is inherently uncertain and will not be resolved by any number of tests, it is preferable from a cost-accuracy perspective to stop early rather than run many expensive tests.

Proposition 1 suggests that we should avoid adopting budget or confidence constraints and instead seek the optimal unconstrained policy. We do not have access to this optimal policy, because we assume that we only have CMI estimates (Section 4.1), so we opt for a simple alternative that avoids per-prediction constraints: we adopt a penalty parameter  $\lambda > 0$ , we make selections at each step according to  $I(\mathbf{y}; \mathbf{x}_i | x_S)/c_i$ , and we terminate the algorithm when  $\arg \max_i I(\mathbf{y}; \mathbf{x}_i | x_S)/c_i < \lambda$ .

Following this approach, we see that a single instantiation of our model can be run with three different stopping criteria: we can use the budget  $k$ , the confidence  $m$ , or the penalty  $\lambda$ . In contrast, prior methods that penalize feature costs required training separately with each  $\lambda$  value [39]. Our claim in Proposition 1 does not apply to our penalized policy with the  $\lambda$  criterion, which is not guaranteed to be optimal, but we find that it leads to improved performance across most datasets.

## 5 Experiments

We now present results from applying our method to several datasets. We refer to our approach as *DIME*<sup>2</sup>(discriminative mutual information estimation) and we explore two data modalities, image and tabular, to evaluate its performance. Our tabular datasets include two medical diagnosis tasks, which represent natural and valuable use cases for DFS; we also use MNIST, which was considered in many prior works [14, 15, 18, 49]. As for our image datasets, we include these because they are studied in several earlier works [39, 41, 51, 57] and represent challenging problems for our method. We show results for our method when evaluated with either the budget-constrained or penalized stopping criteria, and we defer comparison with the confidence-constrained approach to Appendix G. We note again that DIME only needs be trained once to be tested with all three stopping criteria.

In terms of baselines, we compare DIME to both static and dynamic feature selection methods. As a static baseline, we compare to a supervised version of the Concrete Autoencoder (CAE) [7], a state-of-the-art static method that outperformed several dynamic methods in recent work [18]. As dynamic baselines, we consider multiple approaches: first, we compare to the recent discriminative methods that directly predict the CMI’s argmax [15, 18], which we refer to as *Argmax Direct*. Next, as a generative approach, we consider *EDDI* [49], which uses a partial variational autoencoder (PVAE) to sample unknown features. Finally, because EDDI does not scale as well beyond tabular datasets, we compare to probabilistic hard attention (*Hard Attention*) [57], a method that adapts EDDI to work with image data. We omit comparisons to several RL approaches [39, 40, 51] because these are harder to train have not proved to be competitive with our other baselines [15, 18, 57]. Appendix F provides more information about the baseline methods.

### 5.1 Tabular datasets

We first apply our method to three tabular datasets, two of which are medical diagnosis applications. The first task involves predicting whether a patient requires endotracheal intubation for respiratory support (Intubation) in an emergency medicine setting ( $d = 112$ ) [18]. The second one uses cognitive, demographic, and medical history data from the Religious Orders Study and Rush Memory and Aging Project (ROSMAP) [1, 2], two longitudinal aging cohort studies, to predict imminent dementia onset (i.e., a positive diagnosis within the next three years) ( $d = 46$ ). In both scenarios, it is difficult to acquire the complete feature set due to time constraints, thereby showcasing the utility of dynamic feature selection. The third is the standard MNIST digit classification dataset [43], which we formulate as a tabular problem by treating each pixel as an individual feature ( $d = 784$ ). Across all methods, we

<sup>2</sup>Code can be accessed at <https://github.com/suinleelab/DIME>

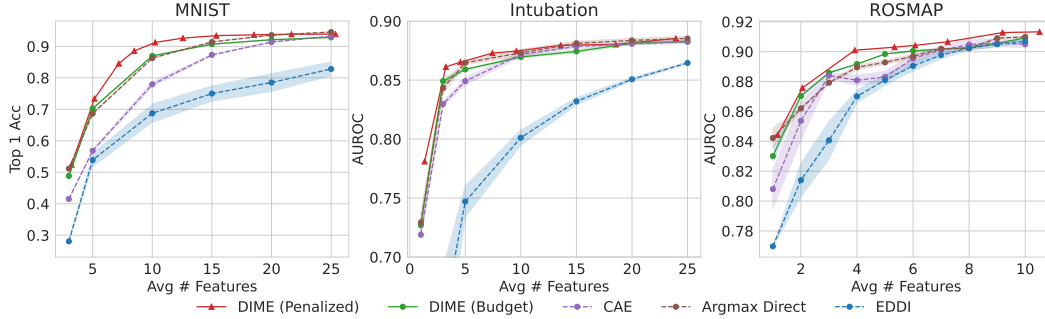


Figure 2: Evaluation with tabular datasets for varying feature acquisition budgets. Results are averaged across 5 trials, and shaded regions indicate the standard error for each method.

use fully connected networks with dropout to reduce overfitting [61]. Classification performance is measured using AUROC for the medical tasks and top-1 accuracy for MNIST. Appendix D provides more details about the datasets, and Appendix E provides more information about the models.

**Uniform feature costs** We first consider the scenario with equal costs for all features. Figure 2 shows the results of applying each method for varying numbers of features. For DIME, we show results when it uses the exact number of features (the budget-constrained approach) and when it uses each number of features *on average* (the penalized approach). DIME with the penalized stopping criterion achieves the best results for nearly all budgets across all three tasks. It performs the best on MNIST, where we are able to achieve above 90% accuracy with only  $\sim 10/784$  features (1.27%). Among the baselines, Argmax Direct is the strongest dynamic method: its performance is nearly identical to DIME with a budget constraint, reflecting the strong similarity between the methods. CAE is a competitive static method, and EDDI usually does not perform well, except for ROSMAP where it approaches the other methods as more features are selected. DIME generally shows the greatest advantage for moderate numbers of features, and the gap reduces as the performance saturates.

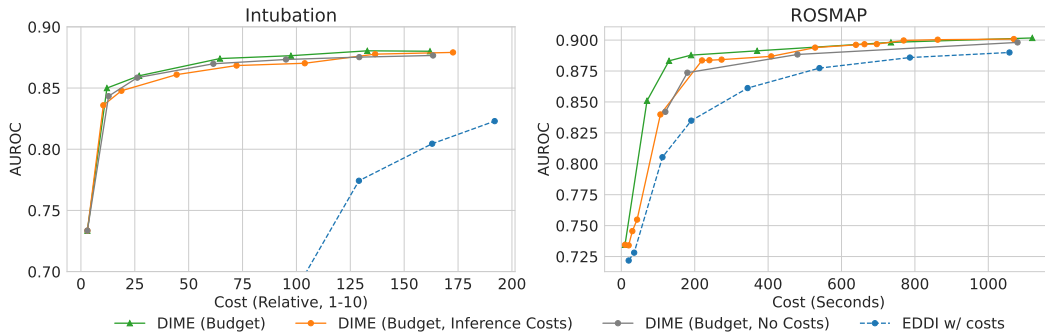


Figure 3: Evaluation with non-uniform feature costs for medical diagnosis tasks. Costs are relative for Intubation and expressed in seconds for ROSMAP. The results show classification performance for varying levels of average feature acquisition cost.

**Non-uniform feature costs** Our CMI estimation approach lets us incorporate non-uniform feature costs into DIME, and we demonstrate this using the Intubation and ROSMAP datasets. For ROSMAP, we use costs expressed as the time required to acquire each feature, and for Intubation we use relative costs estimated by a board-certified physician (Appendix D). For comparisons, EDDI is the only baseline that can be adapted to use non-uniform feature costs as described in Section 4.3. We also compare to two ablations of our approach: (1) using uniform costs during training but the true costs during inference (Budget, Inference Costs), which tests DIME’s robustness to changing feature costs after training; and (2) using uniform costs during both training and inference (Budget, No Costs), which simply demonstrates the importance of using correct costs. All methods are compared here with the budget-constrained stopping criterion.

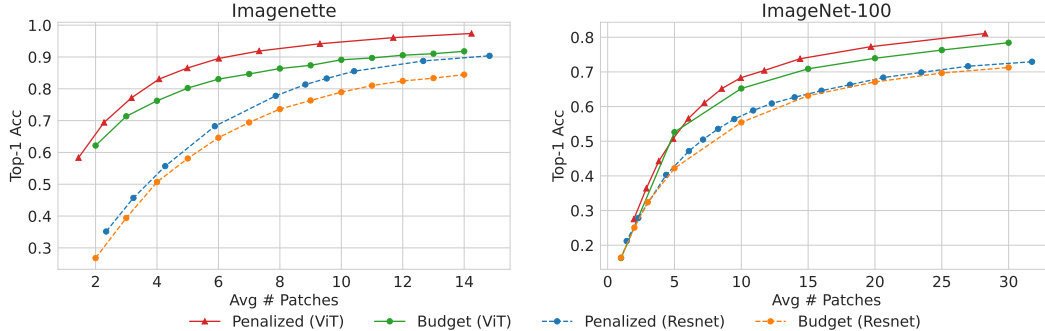


Figure 4: Evaluation of DIME on images with different vision architectures.

Figure 3 shows the results when using non-uniform feature costs. DIME outperforms EDDI by a substantial margin, echoing the earlier results and reflecting the improved CMI estimation with our discriminative approach. Comparing to the variations of DIME, using the true non-uniform costs during both training and inference outperforms both variations, showing that considering costs when making selections is important. The version that uses costs only during inference slightly outperforms ignoring costs on ROSMAP, indicating a degree of robustness to changing feature costs between training and inference, but both versions give similar results on Intubation.

## 5.2 Image datasets

Next, we applied our method to three image classification datasets. The first two are subsets of the standard ImageNet dataset [20], one with 10 classes (Imagenette [37]) and the other with 100 classes (ImageNet-100 [4]). The third is a histopathology classification dataset (MHIST [63]), comprising hematoxylin and eosin (H&E)-stained fixed-size images of colorectal polyps, obtained by extracting diagnostically-relevant image tiles from multiple whole-slide images (WSIs). The task is to predict the histological pattern of each image as either a benign (hyperplastic polyp) or precancerous (sessile serrated adenoma) lesion. WSIs have extremely high resolution and are infeasible to be used directly in any classification task, making them a potential use case for DIME to identify patches most informative to the prediction. The images in all three datasets are  $224 \times 224$ , and we view them as  $d = 196$  patches of size  $16 \times 16$ . The value network predicts the CMI for each patch and the predictor generates class predictions. We explore different architectures for the value and predictor networks, namely ResNets [34] and Vision Transformers (ViTs) [21]. In both cases, we use a shared backbone, with each component having its own output head. Classification performance is measured using top-1 accuracy for both ImageNet subsets, and AUROC for the histopathology task.

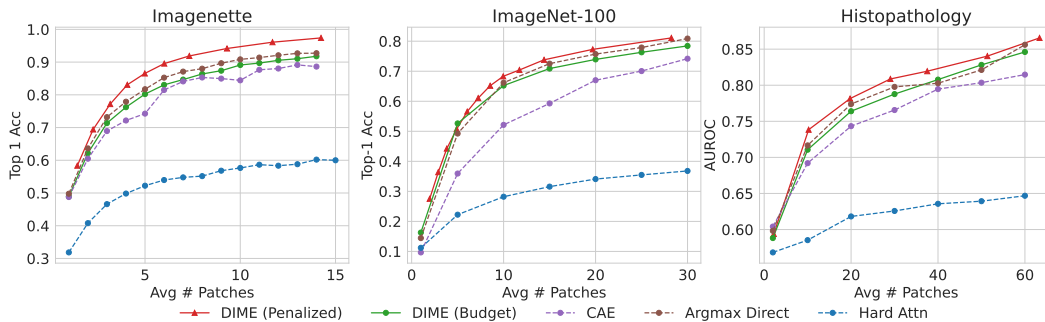


Figure 5: Evaluation with image datasets for varying numbers of average patches selected.

**Exploring modern architectures** Figure 4 compares the performance of ResNet and ViT architectures for the Imagenette and ImageNet-100 datasets. We use DIME to conduct this analysis, because its discriminative approach lets us seamlessly plug in any network architecture. Across both datasets, DIME’s penalized version outperforms the budget-constrained version, and we find that



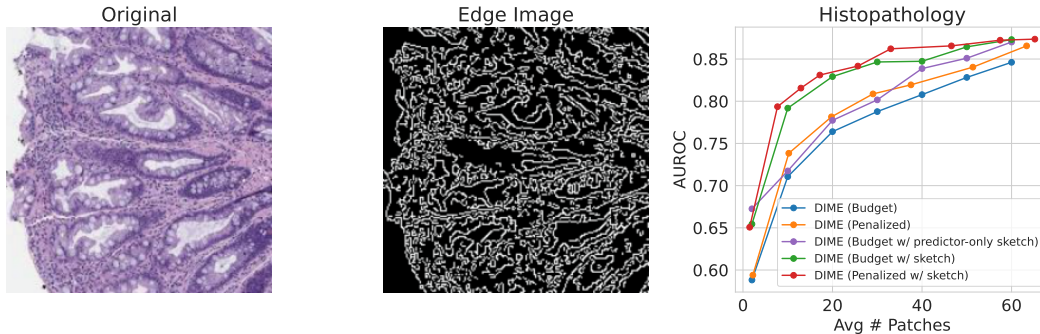


Figure 6: Evaluation of DIME with prior information for histopathology classification. Left: Original MHIST image. Center: Canny edge image. Right: Results for varying number of average patches.

ViTs significantly outperform ResNets. This can be attributed to the ViT’s use of self-attention: this architecture is better suited to handle partial information because it aggregates information from patches anywhere in the image, a property that has made ViTs useful in other applications with partial inputs [38, 53, 59]. Given their superior performance, we use ViTs as backbones in subsequent experiments where possible. This includes DIME, CAE and Argmax Direct, but Hard Attention lacks this flexibility because it relies on a recurrent module to process subsets of image regions.

Figure 5 compares DIME to the baselines across multiple feature budgets. The penalized version outperforms the baselines across all datasets for almost all feature budgets, with the largest gains observed for Imagenette. Notably, we are able to achieve nearly 97% accuracy on Imagenette with only  $\sim 15/196$  patches (7.7%). The Argmax Direct baseline is competitive with DIME’s budget-constrained version, as expected, but the Hard Attention baseline shows a large drop in performance.

**Incorporating prior information** Next, we explored the possibility of incorporating prior information into DIME’s selection process for the histopathology dataset. To simulate informing our selections with a less exact but easily acquirable version of the tissue, we use the Canny edge image [12] as a sketch, which can help generate more valuable selections than a blank image. We use separate ViT backbones for the original and edge images, and we concatenate the resulting embeddings before estimating the CMI or making class predictions (see Appendix E for details). Figure 6 shows example images, along with the results obtained with DIME for various feature budgets. The results show that the prior information is incorporated successfully, leading to improved performance for both the penalized and budget-constrained versions. To verify that the accuracy increase is not solely due to the predictive signal provided by the edge image, we conduct an ablation where the sketch is integrated into the predictor only for a pre-trained and otherwise frozen version of DIME. This middle ground improves upon no prior information, but it generally performs well below the version that uses prior information both when making selections and predictions.

## 6 Conclusion

This work presents DIME, a new approach for dynamic feature selection enabled by estimating the CMI in a discriminative fashion. Our approach involves learned value and predictor networks, trained jointly in an end-to-end fashion with a straightforward regression objective. From a theoretical perspective, we prove that our training approach recovers the exact CMI at optimality. Empirically, DIME is able to accurately estimate the CMI and enables an improved cost-accuracy tradeoff compared to existing methods: it offers a significant improvement over existing generative methods, thereby reducing the need for such models in this setting, and it exceeds the discriminative methods it builds upon [15, 18] by taking advantage of variable feature budgets. Our evaluation considers a range of tabular and image datasets and demonstrates the potential to implement several additions to the classic greedy CMI selection policy: these include allowing non-uniform features costs, variable budgets, and incorporating prior information. The results also show that DIME is robust to higher image resolutions, scales to more classes, and benefits from modern architectures. Future work may focus on promising applications like MRIs and region-of-interest selection within WSIs, using DIME to initialize RL methods, and otherwise accelerating or improving DIME’s training.

## References

- [1] David A Bennett, Julie A Schneider, Zoe Arvanitakis, and Robert S Wilson. Overview and findings from the religious orders study. *Current Alzheimer Research*, 9(6):628–645, 2012.
- [2] David A Bennett, Julie A Schneider, Aron S Buchman, Lisa L Barnes, Patricia A Boyle, and Robert S Wilson. Overview and findings from the rush memory and aging project. *Current Alzheimer Research*, 9(6):646–663, 2012.
- [3] Khaled Abdeljawad, Krishna C Vemulapalli, Charles J Kahi, Oscar W Cummings, Dale C Snover, and Douglas K Rex. Sessile serrated polyp prevalence determined by a colonoscopist with a high lesion detection rate and an experienced pathologist. *Gastrointestinal Endoscopy*, 81(3):517–524, 2015.
- [4] Ambityga. Imagenet100. <https://www.kaggle.com/datasets/ambityga/imagenet100>.
- [5] Jimmy Ba, Volodymyr Mnih, and Koray Kavukcuoglu. Multiple object recognition with visual attention. *arXiv preprint arXiv:1412.7755*, 2014.
- [6] Jimmy Ba, Russ R Salakhutdinov, Roger B Grosse, and Brendan J Frey. Learning wake-sleep recurrent attention models. *Advances in Neural Information Processing Systems*, 28, 2015.
- [7] Muhammed Fatih Balin, Abubakar Abid, and James Zou. Concrete autoencoders: Differentiable feature selection and reconstruction. In *International Conference on Machine Learning*, pages 444–453. PMLR, 2019.
- [8] Nicasia Beebe-Wang, Alex Okeson, Tim Althoff, and Su-In Lee. Efficient and explainable risk assessments for imminent dementia in an aging cohort study. *IEEE Journal of Biomedical and Health Informatics*, 25(7):2409–2420, 2021.
- [9] José M Bernardo. Expected information as expected utility. *The Annals of Statistics*, pages 686–690, 1979.
- [10] Wieland Brendel and Matthias Bethge. Approximating CNNs with bag-of-local-features models works surprisingly well on ImageNet. *arXiv preprint arXiv:1904.00760*, 2019.
- [11] Jie Cai, Jiawei Luo, Shulin Wang, and Sheng Yang. Feature selection in machine learning: A new perspective. *Neurocomputing*, 300:70–79, 2018.
- [12] John Canny. A computational approach to edge detection. *IEEE Transactions on Pattern Analysis and Machine Intelligence*, (6):679–698, 1986.
- [13] Chun-Hao Chang, Ladislav Rampasek, and Anna Goldenberg. Dropout feature ranking for deep learning models. *arXiv preprint arXiv:1712.08645*, 2017.
- [14] Aditya Chattopadhyay, Stewart Slocum, Benjamin D Haeffele, Rene Vidal, and Donald Geman. Interpretable by design: Learning predictors by composing interpretable queries. *IEEE Transactions on Pattern Analysis and Machine Intelligence*, 2022.
- [15] Aditya Chattopadhyay, Kwan Ho Ryan Chan, Benjamin D Haeffele, Donald Geman, and René Vidal. Variational information pursuit for interpretable predictions. *arXiv preprint arXiv:2302.02876*, 2023.
- [16] Yuxin Chen, S Hamed Hassani, Amin Karbasi, and Andreas Krause. Sequential information maximization: When is greedy near-optimal? In *Conference on Learning Theory*, pages 338–363. PMLR, 2015.
- [17] T.M. Cover and J.A. Thomas. *Elements of Information Theory*. Wiley, 2012. ISBN 9781118585771.
- [18] Ian Covert, Wei Qiu, Mingyu Lu, Nayoon Kim, Nathan White, and Su-In Lee. Learning to maximize mutual information for dynamic feature selection. *arXiv preprint arXiv:2301.00557*, 2023.

- [19] Abhimanyu Das and David Kempe. Submodular meets spectral: Greedy algorithms for subset selection, sparse approximation and dictionary selection. *arXiv preprint arXiv:1102.3975*, 2011.
- [20] Jia Deng, Wei Dong, Richard Socher, Li-Jia Li, Kai Li, and Li Fei-Fei. Imagenet: A large-scale hierarchical image database. In *2009 IEEE Conference on Computer Vision and Pattern Recognition*, pages 248–255. Ieee, 2009.
- [21] Alexey Dosovitskiy, Lucas Beyer, Alexander Kolesnikov, Dirk Weissenborn, Xiaohua Zhai, Thomas Unterthiner, Mostafa Dehghani, Matthias Minderer, Georg Heigold, Sylvain Gelly, et al. An image is worth 16x16 words: Transformers for image recognition at scale. *arXiv preprint arXiv:2010.11929*, 2020.
- [22] Gabriel Dulac-Arnold, Ludovic Denoyer, Philippe Preux, and Patrick Gallinari. Datum-wise classification: a sequential approach to sparsity. In *Joint European Conference on Machine Learning and Knowledge Discovery in Databases*, pages 375–390. Springer, 2011.
- [23] Ethan R Elenberg, Rajiv Khanna, Alexandros G Dimakis, and Sahand Negahban. Restricted strong convexity implies weak submodularity. *The Annals of Statistics*, 46(6B):3539–3568, 2018.
- [24] Gabriel Erion, Joseph D Janizek, Carly Hudelson, Richard B Utarnachitt, Andrew M McCoy, Michael R Sayre, Nathan J White, and Su-In Lee. CoAI: Cost-aware artificial intelligence for health care. *medRxiv*, 2021.
- [25] Alton B Farris, Joseph Misdradi, Amitabh Srivastava, Alona Muzikansky, Vikram Deshpande, Gregory Y Lauwers, and Mari Mino-Kenudson. Sessile serrated adenoma: challenging discrimination from other serrated colonic polyps. *The American Journal of Surgical Pathology*, 32(1): 30–35, 2008.
- [26] Jean Feng and Noah Simon. Sparse-input neural networks for high-dimensional nonparametric regression and classification. *arXiv preprint arXiv:1711.07592*, 2017.
- [27] François Fleuret. Fast binary feature selection with conditional mutual information. *Journal of Machine Learning Research*, 5(9), 2004.
- [28] Donald Geman and Bruno Jedynak. An active testing model for tracking roads in satellite images. *IEEE Transactions on Pattern Analysis and Machine Intelligence*, 18(1):1–14, 1996.
- [29] Katharina Glatz, Bobbi Pritt, Dieter Glatz, Arndt Hartmann, Michael J O’Brien, and Hagen Blaszyk. A multinational, internet-based assessment of observer variability in the diagnosis of serrated colorectal polyps. *American Journal of Clinical Pathology*, 127(6):938–945, 2007.
- [30] Daniel Golovin and Andreas Krause. Adaptive submodularity: Theory and applications in active learning and stochastic optimization. *Journal of Artificial Intelligence Research*, 42: 427–486, 2011.
- [31] Isabelle Guyon and André Elisseeff. An introduction to variable and feature selection. *Journal of Machine Learning Research*, 3(Mar):1157–1182, 2003.
- [32] He He, Hal Daumé III, and Jason Eisner. Cost-sensitive dynamic feature selection. In *ICML Inferring Workshop*, 2012.
- [33] He He, Paul Mineiro, and Nikos Karampatziakis. Active information acquisition. *arXiv preprint arXiv:1602.02181*, 2016.
- [34] Kaiming He, Xiangyu Zhang, Shaoqing Ren, and Jian Sun. Deep residual learning for image recognition. In *Proceedings of the IEEE Conference on Computer Vision and Pattern Recognition*, pages 770–778, 2016.
- [35] Weijie He, Xiaohao Mao, Chao Ma, Yu Huang, José Miguel Hernández-Lobato, and Ting Chen. BSODA: a bipartite scalable framework for online disease diagnosis. In *Proceedings of the ACM Web Conference 2022*, pages 2511–2521, 2022.

- [36] Peter Henderson, Riashat Islam, Philip Bachman, Joelle Pineau, Doina Precup, and David Meger. Deep reinforcement learning that matters. In *Proceedings of the AAAI Conference on Artificial Intelligence*, volume 32, 2018.
- [37] FastAI Jeremy Howard. The Imagenette dataset. <https://github.com/fastai/imagenette>.
- [38] Saachi Jain, Hadi Salman, Eric Wong, Pengchuan Zhang, Vibhav Vineet, Sai Vemprala, and Aleksander Madry. Missingness bias in model debugging. In *International Conference on Learning Representations*, 2021.
- [39] Jaromír Janisch, Tomáš Pevný, and Viliam Lisý. Classification with costly features using deep reinforcement learning. In *Proceedings of the AAAI Conference on Artificial Intelligence*, volume 33, pages 3959–3966, 2019.
- [40] Mohammad Kachuee, Orpaz Goldstein, Kimmo Kärkkäinen, Sajad Darabi, and Majid Sarrafzadeh. Opportunistic learning: Budgeted cost-sensitive learning from data streams. In *International Conference on Learning Representations*, 2018.
- [41] Sergey Karayev, Tobias Baumgartner, Mario Fritz, and Trevor Darrell. Timely object recognition. *Advances in Neural Information Processing Systems*, 25, 2012.
- [42] Omer Khalid, Sofyan Radaideh, Oscar W Cummings, Michael J O’Brien, John R Goldblum, and Douglas K Rex. Reinterpretation of histology of proximal colon polyps called hyperplastic in 2001. *World Journal of Gastroenterology*, 15(30):3767, 2009.
- [43] Yann LeCun, Léon Bottou, Yoshua Bengio, and Patrick Haffner. Gradient-based learning applied to document recognition. *Proceedings of the IEEE*, 86(11):2278–2324, 1998.
- [44] Ismael Lemhadri, Feng Ruan, and Rob Tibshirani. Lassonet: Neural networks with feature sparsity. In *International Conference on Artificial Intelligence and Statistics*, pages 10–18. PMLR, 2021.
- [45] Jundong Li, Kewei Cheng, Suhang Wang, Fred Morstatter, Robert P Trevino, Jiliang Tang, and Huan Liu. Feature selection: A data perspective. *ACM Computing Surveys (CSUR)*, 50(6):1–45, 2017.
- [46] Yang Li and Junier Oliva. Active feature acquisition with generative surrogate models. In *International Conference on Machine Learning*, pages 6450–6459. PMLR, 2021.
- [47] Ofir Lindenbaum, Uri Shaham, Erez Peterfreund, Jonathan Svirsky, Nicolas Casey, and Yuval Kluger. Differentiable unsupervised feature selection based on a gated Laplacian. *Advances in Neural Information Processing Systems*, 34:1530–1542, 2021.
- [48] Dennis V Lindley. On a measure of the information provided by an experiment. *The Annals of Mathematical Statistics*, 27(4):986–1005, 1956.
- [49] Chao Ma, Sebastian Tschiatschek, Konstantina Palla, Jose Miguel Hernandez-Lobato, Sebastian Nowozin, and Cheng Zhang. EDDI: Efficient dynamic discovery of high-value information with partial VAE. In *International Conference on Machine Learning*, pages 4234–4243. PMLR, 2019.
- [50] Chao Ma, Sebastian Tschiatschek, Richard Turner, José Miguel Hernández-Lobato, and Cheng Zhang. VAEM: a deep generative model for heterogeneous mixed type data. *Advances in Neural Information Processing Systems*, 33:11237–11247, 2020.
- [51] Andriy Mnih and Karol Gregor. Neural variational inference and learning in belief networks. In *International Conference on Machine Learning*, pages 1791–1799. PMLR, 2014.
- [52] Volodymyr Mnih, Nicolas Heess, Alex Graves, et al. Recurrent models of visual attention. *Advances in Neural Information Processing Systems*, 27, 2014.
- [53] Muhammad Muzammal Naseer, Kanchana Ranasinghe, Salman H Khan, Munawar Hayat, Fahad Shahbaz Khan, and Ming-Hsuan Yang. Intriguing properties of vision transformers. *Advances in Neural Information Processing Systems*, 34, 2021.

- [54] Alfredo Nazabal, Pablo M Olmos, Zoubin Ghahramani, and Isabel Valera. Handling incomplete heterogeneous data using VAEs. *Pattern Recognition*, 107:107501, 2020.
- [55] Andrew Ng and Michael Jordan. On discriminative vs. generative classifiers: A comparison of logistic regression and naive Bayes. *Advances in Neural Information Processing Systems*, 14, 2001.
- [56] Adam Paszke, Sam Gross, Soumith Chintala, Gregory Chanan, Edward Yang, Zachary DeVito, Zeming Lin, Alban Desmaison, Luca Antiga, and Adam Lerer. Automatic differentiation in PyTorch. 2017.
- [57] Samrudhdi B Rangrej and James J Clark. A probabilistic hard attention model for sequentially observed scenes. *arXiv preprint arXiv:2111.07534*, 2021.
- [58] Marc’Aurelio Ranzato. On learning where to look. *arXiv preprint arXiv:1405.5488*, 2014.
- [59] Hadi Salman, Saachi Jain, Eric Wong, and Aleksander Madry. Certified patch robustness via smoothed vision transformers. In *Proceedings of the IEEE/CVF Conference on Computer Vision and Pattern Recognition*, pages 15137–15147, 2022.
- [60] Hajin Shim, Sung Ju Hwang, and Eunho Yang. Joint active feature acquisition and classification with variable-size set encoding. *Advances in Neural Information Processing Systems*, 31, 2018.
- [61] Nitish Srivastava, Geoffrey Hinton, Alex Krizhevsky, Ilya Sutskever, and Ruslan Salakhutdinov. Dropout: a simple way to prevent neural networks from overfitting. *The Journal of Machine Learning Research*, 15(1):1929–1958, 2014.
- [62] Alex Tank, Ian Covert, Nicholas Foti, Ali Shojaie, and Emily B Fox. Neural Granger causality. *IEEE Transactions on Pattern Analysis and Machine Intelligence*, 44(8):4267–4279, 2021.
- [63] Jerry Wei, Arief Suriawinata, Bing Ren, Xiaoying Liu, Mikhail Lisovsky, Louis Vaickus, Charles Brown, Michael Baker, Naofumi Tomita, Lorenzo Torresani, et al. A petri dish for histopathology image analysis. In *Artificial Intelligence in Medicine*, pages 11–24. Springer, 2021.
- [64] Newton ACS Wong, Linda P Hunt, Marco R Novelli, Neil A Shepherd, and Bryan F Warren. Observer agreement in the diagnosis of serrated polyps of the large bowel. *Histopathology*, 55(1):63–66, 2009.

## A Proofs

In this section, we re-state and prove our results from the main text.

### A.1 Estimating conditional mutual information

**Lemma 1.** *When we use the Bayes classifier  $p(\mathbf{y} \mid \mathbf{x}_S)$  as a predictor and  $\ell$  is cross entropy loss, the incremental loss improvement is an unbiased estimator of the CMI for each  $(x_S, \mathbf{x}_i)$  pair:*

$$\mathbb{E}_{\mathbf{y}, \mathbf{x}_i | x_S} [\Delta(x_S, \mathbf{x}_i, \mathbf{y})] = I(\mathbf{y}; \mathbf{x}_i \mid x_S).$$

*Proof.* Consider the expected cross entropy loss given the prediction  $p(\mathbf{y} \mid x_S)$ :

$$\begin{aligned} \mathbb{E}_{\mathbf{y} | x_S} [\ell(p(\mathbf{y} \mid x_S), \mathbf{y})] &= - \sum_{y=1}^K p(\mathbf{y} = y \mid x_S) \log p(\mathbf{y} = y \mid x_S) \\ &= H(\mathbf{y} \mid x_S). \end{aligned}$$

Next, consider the loss given the prediction  $p(\mathbf{y} \mid x_S, x_i)$ , taken in expectation across  $\mathbf{x}_i$  and  $\mathbf{y}$ 's conditional distribution  $p(\mathbf{y}, \mathbf{x}_i \mid x_S)$ :

$$\begin{aligned} \mathbb{E}_{\mathbf{y}, \mathbf{x}_i | x_S} [\ell(p(\mathbf{y} \mid x_S, \mathbf{x}_i), \mathbf{y})] &= \mathbb{E}_{\mathbf{x}_i | x_S} \mathbb{E}_{\mathbf{y} | x_S, \mathbf{x}_i = x_i} [\ell(p(\mathbf{y} \mid x_S, \mathbf{x}_i = x_i), \mathbf{y})] \\ &= \mathbb{E}_{\mathbf{x}_i | x_S} [H(\mathbf{y} \mid x_S, \mathbf{x}_i = x_i)] \\ &= H(\mathbf{y} \mid x_i, \mathbf{x}_i). \end{aligned}$$

We therefore have the following expectation for the incremental loss improvement:

$$\begin{aligned} \mathbb{E}_{\mathbf{y}, \mathbf{x}_i | x_S} [\Delta(x_S, \mathbf{x}_i, \mathbf{y})] &= \mathbb{E}_{\mathbf{y}, \mathbf{x}_i | x_S} [\ell(p(\mathbf{y} \mid x_S), \mathbf{y}) - \ell(p(\mathbf{y} \mid x_S, \mathbf{x}_i), \mathbf{y})] \\ &= H(\mathbf{y} \mid x_S) - H(\mathbf{y} \mid x_S, \mathbf{x}_i) \\ &= I(\mathbf{y}; \mathbf{x}_i \mid x_S). \end{aligned}$$

Thus, the loss improvement  $\Delta(x_S, \mathbf{x}_i, \mathbf{y})$  is an unbiased estimator of the CMI  $I(\mathbf{y}; \mathbf{x}_i \mid x_S)$ .  $\square$

**Theorem 1.** *When  $\ell$  is cross entropy loss, the objectives eq. (2) and eq. (3) are jointly optimized by a predictor  $f(x_S; \theta^*) = p(\mathbf{y} \mid x_S)$  and value network where  $v_i(x_S; \phi^*) = I(\mathbf{y}; \mathbf{x}_i \mid x_S)$  for  $i \in [d]$ .*

*Proof.* Similar to [18], our proof considers both models' optimal predictions for each input. Beginning with the predictor, consider the output given the input  $x_S$ . The selections were made given only  $x_S$ , so observing this input conveys no information about  $\mathbf{y}$  or the remaining features  $\mathbf{x}_{[d] \setminus S}$ . The expected loss is therefore

$$\mathbb{E}_{\mathbf{y} | x_S} [\ell(f(x_S; \theta), \mathbf{y})].$$

Assuming that  $\ell$  is cross entropy loss, we can decompose the expected loss as follows:

$$\begin{aligned} \mathbb{E}_{\mathbf{y} | x_S} [\ell(f(x_S; \theta), \mathbf{y})] &= \sum_{y=1}^K p(\mathbf{y} = y \mid x_S) \log f_y(x_S; \theta) \\ &= \sum_{y=1}^K p(\mathbf{y} = y \mid x_S) \log p(\mathbf{y} = y \mid x_S) \frac{f_y(x_S; \theta)}{p(\mathbf{y} = y \mid x_S)} \\ &= H(\mathbf{y} \mid x_S) + D_{\text{KL}}(p(\mathbf{y} \mid x_S) \parallel f(x_S; \theta)). \end{aligned}$$

Due to the non-negative KL divergence term, we see that the optimal prediction is  $p(\mathbf{y} \mid x_S)$ . We can make this argument for any input  $x_S$ , so we say that the optimal predictor is  $f(x_S; \theta^*) = p(\mathbf{y} \mid x_S)$  for all  $x_S$ . Notably, this argument does not depend on the selection policy: it only requires that the policy has no additional information about the response variable or unobserved features.

Next, we consider the value network while assuming that we use the optimal predictor  $f(\mathbf{x}_S; \theta^*)$ . Given an input  $x_S$ , we once again have no further information about  $\mathbf{y}$  or  $\mathbf{x}_{[d] \setminus S}$ , so the expected loss is taken across the distribution  $p(\mathbf{y}, \mathbf{x}_i \mid x_S)$  as follows:

$$\mathbb{E}_{\mathbf{y}, \mathbf{x}_i \mid x_S} [(v(x_S; \phi) - \Delta(x_S, \mathbf{x}_i, \mathbf{y}))^2].$$

The expected loss can then be decomposed,

$$\begin{aligned} \mathbb{E}_{\mathbf{y}, \mathbf{x}_i \mid x_S} [(v(x_S; \phi) - \Delta(x_S, \mathbf{x}_i, \mathbf{y}))^2] &= \mathbb{E}_{\mathbf{y}, \mathbf{x}_i \mid x_S} [(v(x_S; \phi) - \mathbb{E}_{\mathbf{y}, \mathbf{x}_i \mid x_S} [\Delta(x_S, \mathbf{x}_i, \mathbf{y})])^2] \\ &\quad + \text{Var}(\Delta(x_S, \mathbf{x}_i, \mathbf{y}) \mid x_S), \end{aligned}$$

which reveals that the optimal prediction is  $\mathbb{E}_{\mathbf{y}, \mathbf{x}_i \mid x_S} [\Delta(x_S, \mathbf{x}_i, \mathbf{y})]$ . Following Lemma 1, we know that this is equal to  $I(\mathbf{y}; \mathbf{x}_i \mid x_S)$ . And because we can make this argument for any  $x_S$ , we say that the optimal value network is given by  $v(x_S; \phi^*) = I(\mathbf{y}; \mathbf{x}_i \mid x_S)$ .  $\square$

## A.2 Prior information

Before proving Theorem 2, we first present a preliminary result analogous to Lemma 1.

**Lemma 2.** *When we use the Bayes classifier  $p(\mathbf{y} \mid \mathbf{x}_S, \mathbf{z})$  as a predictor and  $\ell$  is cross entropy loss, the incremental loss improvement is an unbiased estimator of the CMI for each  $(x_S, z, \mathbf{x}_i)$  tuple:*

$$\mathbb{E}_{\mathbf{y}, \mathbf{x}_i \mid x_S} [\Delta(x_S, \mathbf{x}_i, z, \mathbf{y})] = I(\mathbf{y}; \mathbf{x}_i \mid x_S, z).$$

*Proof.* The proof follows the same logic as Lemma 1, where we consider the expected loss before and after incorporating the additional feature  $\mathbf{x}_i$ . The only difference is that each expectation must also condition on  $\mathbf{z} = z$ , so the terms to analyze are

$$\begin{aligned} &\mathbb{E}_{\mathbf{y} \mid x_S, z} [\ell(p(\mathbf{y} \mid x_S, z), \mathbf{y})] \\ &\mathbb{E}_{\mathbf{y}, \mathbf{x}_i \mid x_S, z} [\ell(p(\mathbf{y} \mid x_S, z, \mathbf{x}_i), \mathbf{y})]. \end{aligned}$$

$\square$

We now prove the main result for incorporating prior information.

**Theorem 2.** *When  $\ell$  is cross entropy loss, the objectives in eq. (5) are jointly optimized by a predictor  $f(x_S, z; \theta^*) = p(\mathbf{y} \mid x_S, z)$  and value network where  $v_i(x_S, z; \phi^*) = I(\mathbf{y}; \mathbf{x}_i \mid x_S, z)$  for all  $i \in [d]$ .*

*Proof.* The proof follows the same logic as Theorem 1. For the predictor with input  $x_S$ , we can decompose the expected loss as follows:

$$\mathbb{E}_{\mathbf{y} \mid x_S, z} [\ell(f(x_S, z; \theta), \mathbf{y})] = H(\mathbf{y} \mid x_S, z) + D_{\text{KL}}(p(\mathbf{y} \mid x_S, z) \parallel f(x_S, z; \theta)).$$

This shows that the optimal predictor is  $f(x_S, z; \theta^*) = p(\mathbf{y} \mid x_S, z)$ . Next, assuming we use the optimal predictor, the value network's expected loss can be decomposed as follows:

$$\begin{aligned} \mathbb{E}_{\mathbf{y}, \mathbf{x}_i \mid x_S, z} [(v(x_S, z; \phi) - \Delta(x_S, \mathbf{x}_i, z, \mathbf{y}))^2] &= \mathbb{E}_{\mathbf{y}, \mathbf{x}_i \mid x_S, z} [(v(x_S, z; \phi) - \mathbb{E}_{\mathbf{y}, \mathbf{x}_i \mid x_S, z} [\Delta(x_S, \mathbf{x}_i, z, \mathbf{y})])^2] \\ &\quad + \text{Var}(\Delta(x_S, \mathbf{x}_i, z, \mathbf{y}) \mid x_S, z). \end{aligned}$$

Based on this, Lemma 2 implies that the optimal value network is  $v(x_S, z; \phi^*) = I(\mathbf{y}; \mathbf{x}_i \mid x_S, z)$ .  $\square$

### A.3 Regression version

Before proving our main result for regression models, we first present a preliminary result analogous to Lemma 1.

**Lemma 3.** *When we use the conditional expectation  $\mathbb{E}[\mathbf{y} \mid \mathbf{x}_S]$  as a predictor and  $\ell$  is mean squared error, the incremental loss improvement is an unbiased estimator of the expected reduction in conditional variance for each  $(x_S, \mathbf{x}_i)$  pair:*

$$\begin{aligned}\mathbb{E}_{\mathbf{y}, \mathbf{x}_i | x_S} [\Delta(x_S, \mathbf{x}_i, \mathbf{y})] &= \text{Var}(\mathbf{y} \mid x_S) - \mathbb{E}_{\mathbf{x}_i | x_S} [\text{Var}(\mathbf{y} \mid x_S, \mathbf{x}_i)] \\ &= \text{Var}(\mathbb{E}[\mathbf{y} \mid x_S, \mathbf{x}_i] \mid x_S).\end{aligned}$$

*Proof.* Consider the expected loss given the prediction  $\mathbb{E}[\mathbf{y} \mid x_S]$ :

$$\mathbb{E}_{\mathbf{y} | x_S} \left[ (\mathbb{E}[\mathbf{y} \mid x_S] - \mathbf{y})^2 \right] = \text{Var}(\mathbf{y} \mid x_S).$$

Next, consider the loss given the prediction  $\mathbb{E}[\mathbf{y} \mid x_S, x_i]$ , taken in expectation across  $\mathbf{x}_i$  and  $\mathbf{y}$ 's conditional distribution  $p(\mathbf{y}, \mathbf{x}_i \mid x_S)$ :

$$\begin{aligned}\mathbb{E}_{\mathbf{y}, \mathbf{x}_i | x_S} \left[ (\mathbb{E}[\mathbf{y} \mid x_S, \mathbf{x}_i] - \mathbf{y})^2 \right] &= \mathbb{E}_{\mathbf{x}_i | x_S} \mathbb{E}_{\mathbf{y} | x_S, \mathbf{x}_i = x_i} \left[ (\mathbb{E}[\mathbf{y} \mid x_S, \mathbf{x}_i] - \mathbf{y})^2 \right] \\ &= \mathbb{E}_{\mathbf{x}_i | x_S} [\text{Var}(\mathbf{y} \mid x_S, \mathbf{x}_i)].\end{aligned}$$

We therefore have the following expectation for the incremental loss improvement:

$$\mathbb{E}_{\mathbf{y}, \mathbf{x}_i | x_S} [\Delta(x_S, \mathbf{x}_i, \mathbf{y})] = \text{Var}(\mathbf{y} \mid x_S) - \mathbb{E}_{\mathbf{x}_i | x_S} [\text{Var}(\mathbf{y} \mid x_S, \mathbf{x}_i)].$$

Using the law of total variance, we can simplify this difference as follows:

$$\mathbb{E}_{\mathbf{y}, \mathbf{x}_i | x_S} [\Delta(x_S, \mathbf{x}_i, \mathbf{y})] = \text{Var}(\mathbb{E}[\mathbf{y} \mid x_S, \mathbf{x}_i] \mid x_S).$$

This provides a measure similar to the CMI: it quantifies to what extent different plausible values of  $\mathbf{x}_i$  affect our best estimate for the response variable.  $\square$

We now present our main result for regression models.

**Theorem 3.** *When  $\ell$  is mean squared error, the objectives eq. (2) and eq. (3) are jointly optimized by a predictor  $f(x_S; \theta^*) = \mathbb{E}[\mathbf{y} \mid x_S]$  and value network where for  $i \in [d]$  we have*

$$v(x_S; \phi^*) = \text{Var}(\mathbb{E}[\mathbf{y} \mid x_S, \mathbf{x}_i] \mid x_S).$$

*Proof.* We follow the same proof technique as in Theorem 1. The expected loss for the predictor with input  $x_S$  can be decomposed as follows,

$$\begin{aligned}\mathbb{E}_{\mathbf{y} | x_S} [\ell(f(x_S; \theta), \mathbf{y})] &= \mathbb{E}_{\mathbf{y} | x_S} \left[ (f(x_S; \theta) - \mathbf{y})^2 \right] \\ &= \mathbb{E}_{\mathbf{y} | x_S} \left[ (f(x_S; \theta) - \mathbb{E}[\mathbf{y} \mid x_S])^2 \right] + \text{Var}(\mathbf{y} \mid x_S),\end{aligned}$$

which shows that the optimal predictor network is  $f(x_S; \theta^*) = \mathbb{E}[\mathbf{y} \mid x_S]$ . Assuming we use the optimal predictor, the expected loss for the value network can then be decomposed as

$$\begin{aligned}\mathbb{E}_{\mathbf{y}, \mathbf{x}_i | x_S} \left[ (v(x_S; \phi) - \Delta(x_S, \mathbf{x}_i, \mathbf{y}))^2 \right] &= \mathbb{E}_{\mathbf{y}, \mathbf{x}_i | x_S} \left[ (v(x_S; \phi) - \mathbb{E}_{\mathbf{y}, \mathbf{x}_i | x_S} [\Delta(x_S, \mathbf{x}_i, \mathbf{y})])^2 \right] \\ &\quad + \text{Var}(\Delta(x_S, \mathbf{x}_i, \mathbf{y}) \mid x_S),\end{aligned}$$

which shows that the optimal value network prediction is  $\mathbb{E}_{\mathbf{y}, \mathbf{x}_i | x_S} [\Delta(x_S, \mathbf{x}_i, \mathbf{y})]$ . Lemma 3 lets us conclude that the optimal value network is therefore  $v(x_S; \phi^*) = \text{Var}(\mathbb{E}[\mathbf{y} \mid x_S, \mathbf{x}_i] \mid x_S)$ .  $\square$



#### A.4 Allowing a variable feature budget

We first re-state our informal claim, and then introduce notation required to show a formal version.

**Proposition 1.** *(Informal) For any feature budget  $k$ , the best policy to achieve this budget on average achieves lower loss than the best policy with a per-prediction budget constraint. Similarly, for any confidence level  $m$ , the best policy to achieve this confidence on average achieves lower cost than the best policy with a per-prediction confidence constraint.*

In order to account for a policy’s stopping criterion, we generalize our earlier notation so that policies are functions of the form  $\pi(x_S) \in \{0\} \cup [d]$ , and we say a policy terminates (or stops selecting new features) when  $\pi(x_S) = 0$ . Given an input  $x$ , we let  $S(\pi, x) \subseteq [d]$  denote the set of indices selected upon termination. The cost for this prediction is  $c(\pi, x) = \sum_{i \in S(\pi, x)} c_i$ , and there is also a notion of expected loss  $\ell(\pi, x)$  that we define as follows:

$$\ell(\pi, x) = \mathbb{E}_{\mathbf{y}|x_{S(\pi, x)}}[\ell(f(x_{S(\pi, x)}), \mathbf{y})]. \quad (6)$$

For example, if  $\ell$  is cross entropy loss and we use the Bayes classifier  $f(x_S) = p(\mathbf{y} | x_S)$ , we have  $\ell(\pi, x) = H(\mathbf{y} | x_S)$ ; due to this interpretation of the expected loss, we refer to constraints on  $\ell(\pi, x)$  as *confidence constraints*. For example, Chattopadhyay et al. [15] suggests continuing to select features until  $H(\mathbf{y} | x_S) \leq m$  for a confidence level  $m$ . In comparing policies, we must consider the tradeoff between accuracy and feature cost, and we have two competing objectives – the average loss and the average cost:

$$\ell(\pi) = \mathbb{E}[\ell(\pi, \mathbf{x})] \quad c(\pi) = \mathbb{E}[c(\pi, \mathbf{x})]. \quad (7)$$

Now, there are three types of policies we wish to compare: (1) those that adopt a budget constraint for each prediction, (2) those that adopt a confidence constraint for each prediction, and (3) those with no constraints. These classes of selection policies are defined as follows:

1. (Budget-constrained) These policies adopt a budget  $k$  that must be respected for each input  $x$ . That is, we have  $c(\pi, x) \leq k$  for all  $x$ . This can be ensured by terminating the policy when the budget is exactly satisfied [18, 49, 57] or when there are no more candidates that will not exceed the budget. Policies of this form are said to belong to the set  $\Pi_k$ .
2. (Confidence constrained) These policies adopt a minimum confidence  $m$  that must be respected for each input  $m$ . That is, we must have  $\ell(\pi, x) \leq m$  for all  $x$ . Technically, we may not be able to guarantee this for all predictions due to inherent uncertainty, so we can instead keep making predictions as long as the expected loss exceeds  $m$  [15]. Policies of this form are said to belong to the set  $\Pi_m$ .
3. (Unconstrained) These policies have no per-prediction constraints on the feature cost or expected loss. These policies are said to belong to the set  $\Pi$ , where we have  $\Pi_k \subseteq \Pi$  and  $\Pi_m \subseteq \Pi$ .

With these definitions in place, we now present a more formal version of our claim.

**Proposition 2.** *(Formal) For any average feature cost  $k$ , the best unconstrained policy achieves lower expected loss than the best budget-constrained policy:*

$$\min_{\pi \in \Pi: c(\pi) \leq k} \ell(\pi) \leq \min_{\pi \in \Pi_k} \ell(\pi). \quad (8)$$

*Similarly for any average confidence level  $m$ , the best unconstrained policy achieves lower expected cost than the best confidence-constrained policy:*

$$\min_{\pi \in \Pi: \ell(\pi) \leq m} c(\pi) \leq \min_{\pi \in \Pi_m} c(\pi). \quad (9)$$

In other words, for any desired average feature cost or confidence level, it cannot help to adopt that level as a per-prediction constraint. The best policy to achieve these levels *on average* can violate the constraint for some predictions, and as a result provide either a lower average cost or expected loss.

*Proof.* The proof of this claim relies on the fact that  $\Pi_k \subseteq \Pi$  and  $\Pi_m \subseteq \Pi$ . It is easy to see that  $\Pi_k \subseteq \{\pi \in \Pi : c(\pi) \leq k\}$ . This implies the inequality in eq. (8) because the right-hand side takes the minimum over a smaller set of policies. Similarly, it is easy to see that  $\Pi_m \subseteq \{\pi \in \Pi : \ell(\pi) \leq m\}$ , which implies the inequality in eq. (9).  $\square$

## B Predictor suboptimality

Consider a feature subset  $x_S$  where the ideal prediction from the Bayes classifier is  $p(\mathbf{y} | x_S)$ , but the learned classifier instead outputs  $q(\mathbf{y} | x_S)$ . The incorrect prediction can result in a skewed loss, which then provides incorrect labels to the value network  $v(x_S; \phi)$ . Specifically, the expected loss assuming many data points  $(\mathbf{x}, \mathbf{y})$  such that  $\mathbf{x}_S = x_S$  becomes

$$\mathbb{E}_{\mathbf{y}|x_S}[\ell(q(\mathbf{y} | x_S), \mathbf{y})] = H(\mathbf{y} | x_S) + D_{\text{KL}}(p(\mathbf{y} | x_S) || q(\mathbf{y} | x_S)). \quad (10)$$

The loss is therefore higher on average than it should be given the Bayes classifier, with the extra loss being equal to the KL divergence between the ideal and actual predictions. However, this does not imply that  $v(x_S; \phi)$  systematically overestimates the CMI, because its labels are based on the expected loss *reduction*.

Consider that the above situation with incorrect predictions occurs not only for  $x_S$ , but also for all values of  $\mathbf{x}_i$ : that is, the classifier outputs  $q(\mathbf{y} | x_S, x_i)$  rather than  $p(\mathbf{y} | x_S, x_i)$  for each value  $x_i$ . Now, the expected loss reduction is the following:

$$\begin{aligned} \mathbb{E}_{\mathbf{y}, \mathbf{x}_i | x_S}[\Delta(x_S, \mathbf{x}_i, \mathbf{y})] &= I(\mathbf{y}; \mathbf{x}_i | x_S) + D_{\text{KL}}(p(\mathbf{y} | x_S) || q(\mathbf{y} | x_S)) \\ &\quad - \mathbb{E}_{\mathbf{x}_i | x_S}[D_{\text{KL}}(p(\mathbf{y} | x_S, \mathbf{x}_i) || q(\mathbf{y} | x_S, \mathbf{x}_i))]. \end{aligned} \quad (11)$$

This implies that given infinite data and a value network that perfectly optimizes its objective, the learned CMI estimates are biased according to a *difference* in KL divergence terms. Notably, the difference can be either positive or negative, so the CMI estimates can be incorrect in either direction. And intuitively, the bias shrinks to zero as the classifier approaches  $p(\mathbf{y} | x_S)$  for all predictions.

## C Training algorithm

The following algorithm summarizes our learning approach, where we jointly train the predictor and value networks according to the objectives in eq. (2) and eq. (3). We implemented it in PyTorch [56] using PyTorch Lightning.<sup>3</sup> Note that the algorithm requires a dataset of fully observed  $\mathbf{x}$  samples with corresponding labels  $\mathbf{y}$ .

---

**Algorithm 1:** Training algorithm

---

**Input:** Data distribution  $p(\mathbf{x}, \mathbf{y})$ , learning rate  $\gamma$ , budget  $k$ , exploration  $\epsilon \in (0, 1)$ , costs  $c \in \mathbb{R}_+^d$

**Output:** Predictor  $f(\mathbf{x}_S; \theta)$ , value network  $v(\mathbf{x}_S; \phi)$

```
// Prepare models
initialize  $v(\mathbf{x}_S; \phi)$ , pre-train  $f(\mathbf{x}_S; \theta)$  with random masks

while not converged do
  // Initialize variables
  initialize  $S = \{\}$ ,  $\mathcal{L}_\theta = 0$ ,  $\mathcal{L}_\phi = 0$ 
  sample  $x, y \sim p(\mathbf{x}, \mathbf{y})$ 

  // Initial prediction
  calculate  $\hat{y}_{\text{prev}} = f(x_{\{\}}; \theta)$ 
  update  $\mathcal{L}_\theta \leftarrow \mathcal{L}_\theta + \ell(\hat{y}_{\text{prev}}, y)$ 

  while  $\sum_{i \in S} c_i \leq k$  do
    // Determine next selection
    calculate  $I = v(x_S; \phi)$ 
    set  $j = \arg \max_{i \notin S} I_i / c_i$  with probability  $1 - \epsilon$ , else sample  $j$  from  $[d] \setminus S$ 

    // Update predictor loss
    update  $S \leftarrow S \cup j$ 
    calculate  $\hat{y} = f(x_S; \theta)$ 
    update  $\mathcal{L}_\theta \leftarrow \mathcal{L}_\theta + \ell(\hat{y}, y)$ 

    // Update value loss
    calculate  $\Delta = \ell(\hat{y}_{\text{prev}}, y) - \ell(\hat{y}, y)$ 
    update  $\mathcal{L}_\phi \leftarrow \mathcal{L}_\phi + (I_j - \Delta)^2$ 
    set  $\hat{y}_{\text{prev}} = \hat{y}$ 
  end

  // Gradient step
  update  $\theta \leftarrow \theta - \gamma \nabla_\theta \mathcal{L}_\theta$ ,  $\phi \leftarrow \phi - \gamma \nabla_\phi \mathcal{L}_\phi$ 
end
```

---

Algorithm 1 is simplified to omit several details that we implement in practice. These details are discussed below.

**Masked pre-training** When pre-training the predictor  $f(\mathbf{x}_S; \theta)$ , we sample feature subsets as follows: we first sample a cardinality  $\{0, \dots, d\}$  uniformly at random, and we then sample the members of the subset at random. This distribution ensures even coverage of different subset sizes  $|S|$ , whereas treating each feature’s membership as an independent Bernoulli variable biases the subsets towards a specific size.

**Minibatching** As is conventional in deep learning, we calculate gradients in parallel for multiple inputs. In Algorithm 1, this means that we take gradient steps calculated over (1) multiple data samples  $(\mathbf{x}, \mathbf{y})$  and (2) multiple feature budgets.

**Learning rate schedule** Rather than train with a fixed learning rate  $\gamma > 0$ , we reduce its value over the course of training. To avoid setting a precise number of epochs for each dataset, we decay the learning rate when the loss reaches a plateau, and we perform early stopping when the learning rate

---

<sup>3</sup><https://www.pytorchlightning.ai>

is sufficiently low. The initial learning rate depends on the architecture, but we use values similar to those used for conventional training (e.g., ViTs require a lower learning rate than CNNs or MLPs).

**Annealing exploration probability** Setting a large value for  $\epsilon$  helps encourage exploration, but at inference time we set  $\epsilon = 0$ . To avoid the mismatch between these settings, we sometimes anneal  $\epsilon$  towards zero over the course of training. Specifically, we train the model with a sequence of  $\epsilon$  values, warm-starting each model with the output from the previous value.

**Parameter sharing** As mentioned in Section 4, we sometimes share parameters between the predictor and value network. We implement this via a shared backbone, e.g., a sequence of self-attention layers in a ViT [21]. The backbone is initialized via the predictor pre-training with random masks, and it is then used for both  $f(\mathbf{x}_S; \theta)$  and  $v(\mathbf{x}_S; \phi)$  with separate output heads for each one.

**Scaling value network outputs** To learn the optimal value network outputs, it is technically sufficient to let the network make unconstrained, real-valued predictions. However, given that the true CMI values are non-negative, or  $I(\mathbf{y}; \mathbf{x}_i | x_S) \geq 0$  for all  $(x_S, \mathbf{x}_i)$ , it is sensible to constrain the predictions: for example, we can apply a softplus output activation. Similarly, we know that the true CMI values are upper bounded by the current prediction entropy  $H(\mathbf{y} | x_S)$  [17]. These simultaneous bounds can be summarized as follows:

$$0 \leq I(\mathbf{y}; \mathbf{x}_i | x_S) \leq H(\mathbf{y} | x_S).$$

To enforce both inequalities, we apply a sigmoid operation to the unconstrained value network prediction  $v(x_S; \phi)$ , and we multiply this by the empirical prediction entropy from  $f(x_S; \theta)$ . An ablation showing the effect of this approach is in Figure 9.

**Prior information** We found that an issue with using prior information (as discussed in Section 4.2) is overfitting to  $\mathbf{z}$ . This is perhaps unsurprising, particularly when  $\mathbf{z}$  is high-dimensional, because the same input is used repeatedly with different feature subsets  $\mathbf{x}_S$  and the same label  $\mathbf{y}$ . To mitigate this, we applied the following simple fix: for the separate network that processes the prior variable  $\mathbf{z}$ , we detached gradients when using the learned representation to make classifier predictions, so that gradients are propagated only for the value network’s CMI predictions. An ablation demonstrating this approach is in Figure 14.

**Inference time.** At inference time, we follow a similar procedure as in Algorithm 1 but with  $\epsilon = 0$ , so that we always make the most valuable selection. In terms of stopping criteria for making a prediction, we explore multiple approaches, as discussed in Section 4.3: (1) a budget-constrained approach with parameter  $k$ , (2) a confidence constrained approach with parameter  $m$ , and (3) a penalized approach with parameter  $\lambda$ . Our results are generated by evaluating a single learned policy with several values for each of these parameters. The range of reasonable values for the confidence parameter  $m$  and penalty parameter  $\lambda$  depend on the dataset, so these are tuned by hand.

## D Datasets

This section provides details about the datasets used in our experiments. The size of each dataset is summarized in Table 1.

Table 1: Summary of datasets used in our experiments.

Dataset	# Features	# Feature Groups	# Classes	# Samples
MNIST	784	–	10	60,000
Intubation	112	35	2	65,515
ROSMAP	46	43	2	13,438
ImageNette	50,176	196	10	13,395
ImageNet-100	50,176	196	100	135,000
Histopathology	50,176	196	2	3152

**MNIST** This is the standard digit classification dataset [43]. We downloaded it with PyTorch and used the standard train and test splits, with 10,000 training samples held out as a validation set.

**Intubation** This is a privately curated dataset from a university medical center, gathered over a 13-year period (2007-2020). Our goal is to predict which patients require respiratory support upon arrival in the emergency department. We selected 112 pre-hospital clinical features including dispatch information (injury date, time, cause, and location), demographic information (age, sex), and pre-hospital vital signs (blood pressure, heart rate, respiratory rate). The outcome is defined based on whether a patient received respiratory support, including both invasive (intubation) and non-invasive (BiPap) approaches. We excluded patients under the age of 18, and because many features represent one-hot encodings for categorical variables, we grouped them into 35 feature groups. Feature acquisition costs were obtained by having a board-certified emergency physician estimate the relative cost of obtaining each feature. The dataset is not publicly available due to patient privacy concerns.

**ROSMAP** The Religious Order Study (ROS) and Memory Aging Project (MAP) [1, 2] are complementary epidemiological studies that enroll participants to study dementia. ROS is a longitudinal study that enrolls clergy without known dementia from across the United States, including Catholic nuns, priests, and brothers aged 65 years and older. Participants agree to annual medical and psychological evaluation and pledge their brain for donation. MAP is a longitudinal study that enrolls participants encompassing a wider community from 40 continuous care retirement facilities around the Chicago metropolitan area. Participants are without known dementia and agree to annual clinical evaluation and donation of brain, spinal cord and muscle after death. While entering the study, participants share demographic information (e.g. age, sex) and also provide their blood samples for genotyping. At each annual visit, their medical information is updated and they take a series of cognitive tests, which generate multiple measurements over time. This results in 46 different variables, grouped into 43 feature groups to account for one-hot encodings. The task is to predict dementia onset within the next three years given the current medical information and no prior history of dementia. In total, the data contains 3,194 individuals with between 1 and 23 annual visits. Following the preprocessing steps used in [8], we applied a four-year sliding window over each sample, thereby generating multiple samples per participant. Each sample is split into an input window consisting of the current year visit  $t$  and a prediction window of the next three years ( $t + 1, t + 2, t + 3$ ). To avoid overlap between the training, validation, or testing sets, we ensured that all samples from a single individual fell into only one of the data splits. Feature acquisition costs expressed in terms of time taken were borrowed from [8] for the cognitive tests and rough estimates were assigned to the remaining features using prior knowledge. We discarded the genotypic feature (APOE e4 allele) from the feature set since it is highly predictive of dementia and it is difficult to assign an appropriate cost. The dataset can be accessed at <https://dss.niagads.org/cohorts/religious-orders-study-memory-and-aging-project-rosmap/>.

**ImageNette and ImageNet-100** These are both subsets of the standard ImageNet dataset [20]. ImageNette contains 10 classes and was downloaded using the Fast.ai deep learning library [37], ImageNet-100 contains 100 classes and was downloaded from Kaggle [4], and in both cases we split the images to obtain train, validation and test splits. Images were resized to  $224 \times 224$  resolution for both architectures we explored, ResNets [34] and ViTs [21].

**MHIST** The MHIST (**minimalist histopathology**) [63] dataset is an image classification dataset comprising 3,152 hematoxylin and eosin (H&E)-stained Formalin Fixed Paraffin-Embedded (FFPE) fixed-size images of colorectal polyps from patients at Dartmouth-Hitchcock Medical Center (DHMC). The task is to perform binary classification between hyperplastic polyps (HPs) and sessile serrated adenomas (SSAs), which is a challenging prediction task with significant variation in inter-pathologist agreement [3, 25, 29, 42, 64]. HPs are typically benign, while SSAs are precancerous lesions that can turn into cancer if not treated promptly. The fixed-size images were obtained by scanning 328 whole-slide images and then extracting regions of size  $224 \times 224$  representing diagnostically-relevant regions of interest for HPs or SSAs. For the ground truth, each image was assigned a gold-standard label determined by the majority vote of seven board-certified gastrointestinal pathologists at the DHMC. The dataset can be accessed by filling out the form at <https://bmirds.github.io/MHIST/>.

## E Models

Here, we briefly describe the types of models used for each dataset. The exploration probability  $\epsilon$  for all models is set to 0.05 at the start with an annealing rate of 0.2.

**Tabular datasets** For all the tabular datasets, we use multilayer perceptrons (MLPs) with two hidden layers and ReLU non-linearity. We use 128 neurons in the hidden layers for the ROSMAP and Intubation datasets, and 512 neurons for MNIST. The initial learning rate is set to  $10^{-3}$  at the start and we also use dropout with probability 0.3 in all layers to reduce overfitting [61]. The value and predictor networks use separate but identical network architectures. The networks are trained on a NVIDIA RTX 2080 Ti GPU with 12GB of memory.

**Image datasets: ResNet** We use a shared ResNet-50 backbone [34] for the predictor and value networks. The final representation from the backbone has shape  $7 \times 7$ , and the output heads for each network are specified as follows. The predictor head contains a Conv  $\rightarrow$  Batch Norm  $\rightarrow$  ReLU sequence followed by global average pooling and a fully connected layer. The value network head consists of an upsampling block with a transposed convolutional layer, followed by a  $1 \times 1$  convolution and a sigmoid to scale the predictions (see Appendix C). The learning rate starts at  $10^{-5}$ , and the networks are trained on a NVIDIA RTX 2080 Ti GPU with 12GB of memory.

**Image datasets: ViT** We use a shared ViT backbone (`vit_small_patch16_224`) [21] for the predictor and value networks. We use ViT and ResNet backbones having a similar number of parameters for a fair comparison: ResNet-50 has approximately 23M parameters, and ViT-Small has 22M parameters. The predictor head contains a linear layer applied to the class token, and the value network head contains a linear layer applied to all tokens except for the class token, followed by a sigmoid function. When incorporating prior information, a separate ViT backbone is used for both the predictor and value networks to generate an embedding, which is then concatenated with the masked image embedding to get either the predicted CMIs or the class prediction. The learning rate starts at  $10^{-5}$ , and the networks are trained on a NVIDIA Quadro RTX 6000 GPU with 24GB of memory.

## F Baselines

Here, we provide more details here on our baseline methods.

**Concrete autoencoder** This is a static feature selection method that optimizes a differentiable selection module within a neural network [7]. The layer can be added at the input of any architecture, so we use this method for both tabular and image datasets. The original work suggested training with an exponentially decayed temperature and a hand-tuned number of epochs, but we use a different approach to minimize the tuning required for each dataset: we train with a sequence of temperature values, and we perform early stopping for each one based on the validation loss. We return the features that are selected after training with the lowest temperature, and we evaluate them by training a model from scratch with only those features provided.

**EDDI** This is a dynamic feature selection method that relies on a generative model to sample the unobserved features [49]. We implement a PVAE to sample the unknown features, and these samples are used to estimate the CMI for candidate features at each selection step. We separately implement a classifier that makes predictions with arbitrary feature sets, similar to the one obtained after masked pre-training in Algorithm 1. We use this method only for our tabular datasets, as the PVAE is not expected to work well for images, and the computational cost at inference time is relatively high.

**Probabilistic hard attention** This method extends EDDI to work for images by imputing unobserved features within a lower dimensional, learned feature space [57]. To ensure that the method operates on the same image regions as DIME, we implemented a feature extractor that separately computes embeddings for non-overlapping  $14 \times 14$  patches, similar to a ViT [21] or bag-of-features model [10]. Specifically, our extractor consists of a single  $16 \times 16$  convolutional layer, followed by a series of  $1 \times 1$  convolutions. The features from each patch are aggregated by a recurrent module, and we retain the same structure used in the original implementation.

**Argmax Direct** This is a dynamic feature selection method that directly estimates the feature index with maximum CMI. It is based on two concurrent works whose main difference is how gradients are calculated for the selector network [15, 18]; for simplicity, we only explore the technique based on the Concrete distribution from [18]. As a discriminative method, this baseline allows us to use arbitrary architectures and is straightforward to apply with either tabular or image datasets.

## G Additional results

Here, we present the results of several additional experiments and ablations on the different datasets.

Figure 7 shows the prediction calibration of the predictor network by plotting DIME’s performance at different levels of confidence for a specific budget of  $k = 15$ , along with the density of the samples at those confidence levels across multiple datasets. This shows that the predictor network is well-calibrated and does not systematically overestimate or underestimate its predicted probabilities. Proper calibration is important to achieve accurate loss values, because these are then used to train the value network (see eq. (3)).

Figure 8 shows the calibration of the predicted CMIs by the value network for both a tabular and image dataset by plotting the difference in entropy or losses against the predicted CMI. A linear trend showcases that the CMIs predicted by the value network align well with the difference in either the entropy or the loss. Since we do not have ground truth CMI values to evaluate the accuracy of our value network, this serves a viable alternative for real-world datasets, and we can verify that the CMI predictions correctly represent the expected reduction in either loss or entropy.

Figure 9 shows the effect of constraining the predicted CMIs using the current prediction entropy, as described in Appendix C. Without the constraint, there are some samples that have unrealistically high CMIs which are greater than the prediction entropy. After applying the sigmoid activation on the value network predictions, this issue is corrected.

Figure 10 shows multiple trials for the penalized policy on the tabular datasets. This provides a simple way to represent variability between trials when we cannot precisely control the budget between independent policies. Similarly, Figure 11 and Figure 12 show multiple trials while considering non-uniform feature costs. The relative results stay the same across all trials.

Figure 13 shows the confidence distribution of full input predictions in the tabular datasets. Across all datasets, we observe that the model has high confidence in many of the samples, but there are some that remain uncertain even after observing all the features. This provides motivation for using the penalized approach, because a confidence-constrained approach could suffer here by expending the entire feature acquisition budget only to remain at high uncertainty.

Figure 14 shows the effectiveness of detaching gradients for the predictor network of the sketch  $\mathbf{z}$  in the histopathology dataset, as described in Appendix C. The penalized policy performs much better when we propagate gradients only for CMI predictions, which we attribute to reduced overfitting to the prior information. Figure 15 compares the confidence-constrained stopping criterion with the other two approaches (penalized and budget-constrained) for two of the image datasets.

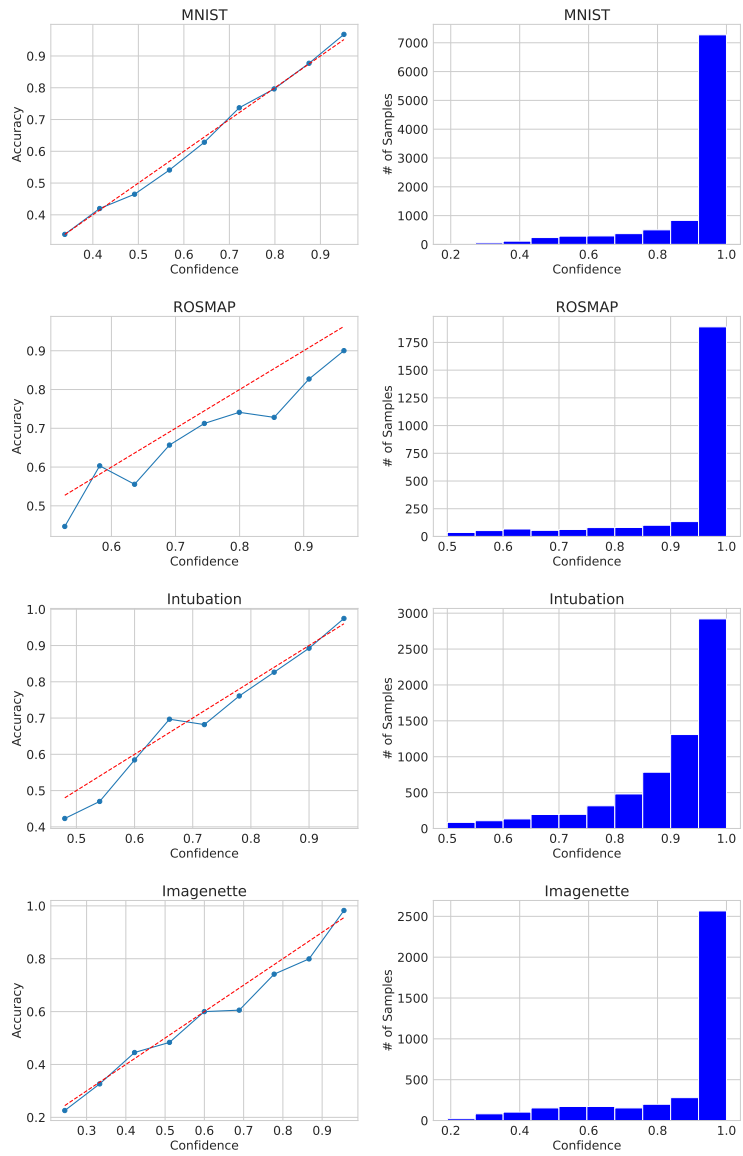


Figure 7: Evaluation of prediction calibration for a fixed budget of  $k = 15$ . The left column shows the prediction calibration of the predictor network by plotting the accuracy for different confidence levels. The right column shows the distribution of confidences across all samples.



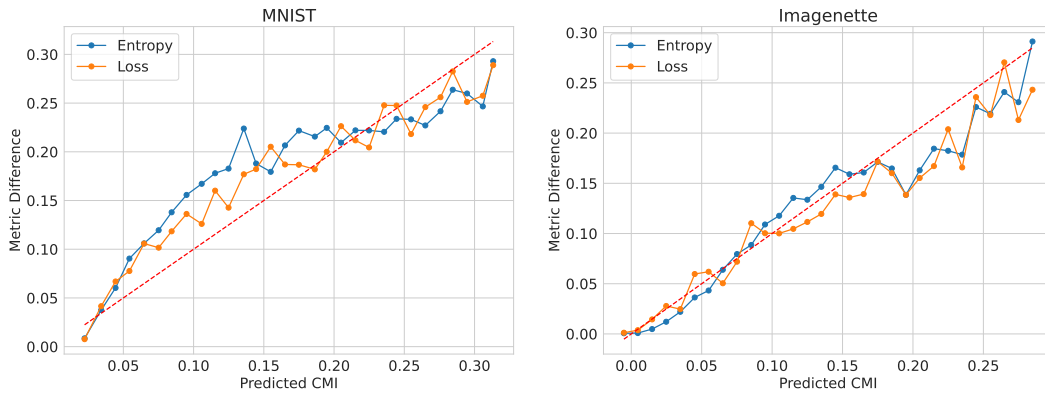


Figure 8: Evaluation of CMI calibration. The x-axis shows different values for the predicted CMI throughout the selection process, and the y-axis shows the reduction in either loss or entropy after the corresponding feature is selected.

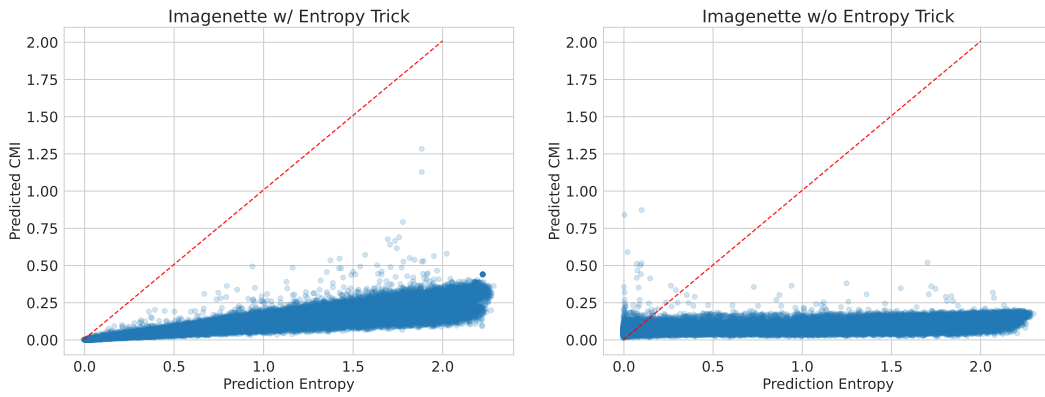


Figure 9: Predicted CMI with and without the entropy trick to scale value network outputs.

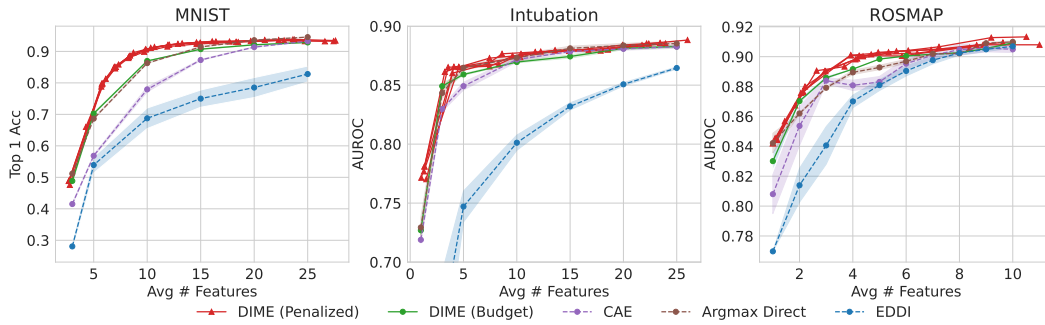


Figure 10: Multiple trials using the penalized policy for tabular datasets. DIME remains the best method across five independent trials.

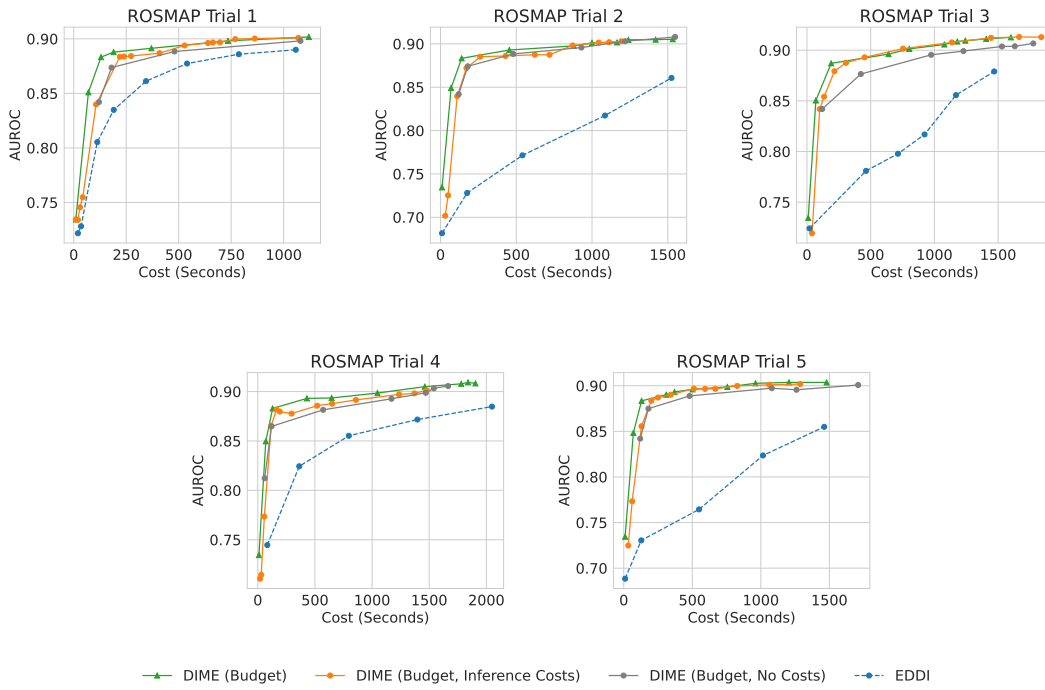


Figure 11: Multiple trials when using non-uniform feature costs for ROSMAP.

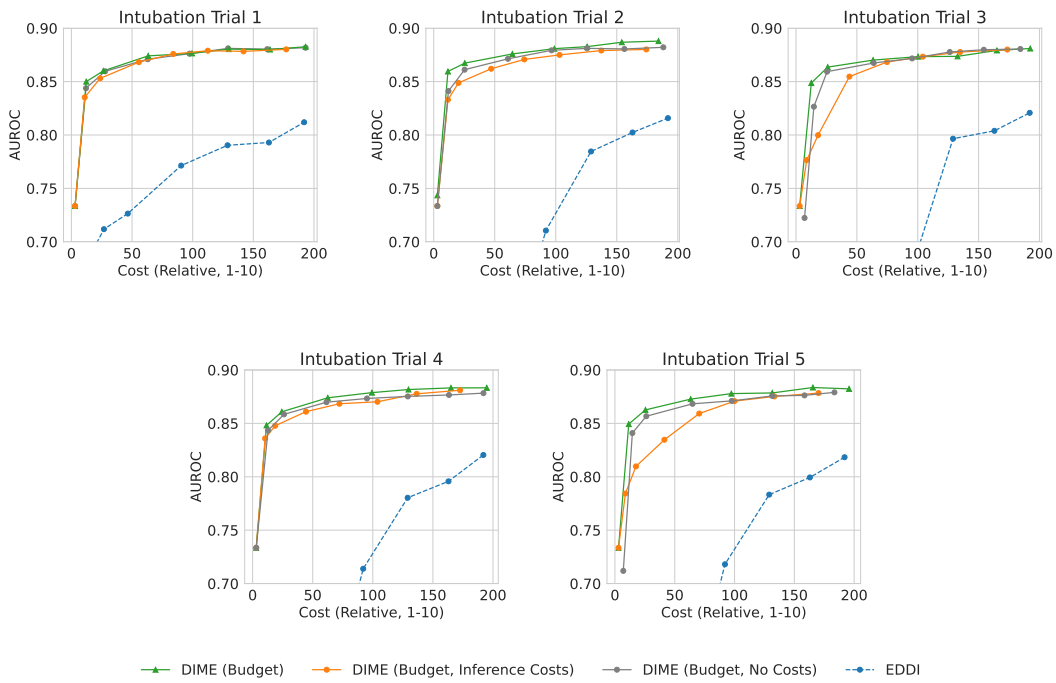


Figure 12: Multiple trials when using non-uniform feature costs for Intubation.

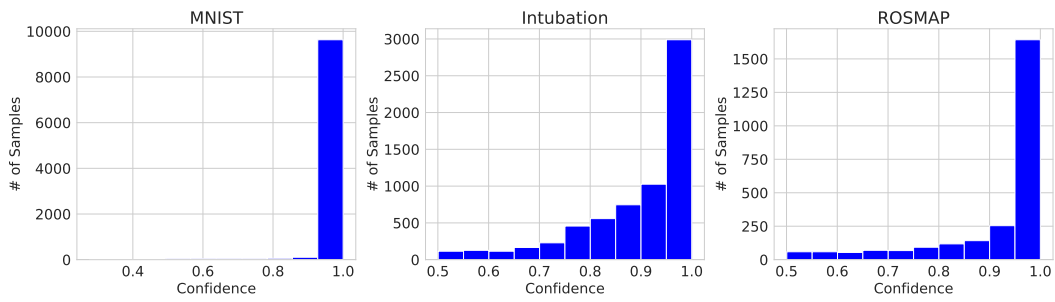


Figure 13: Confidence distribution on full-input predictions across the tabular datasets.

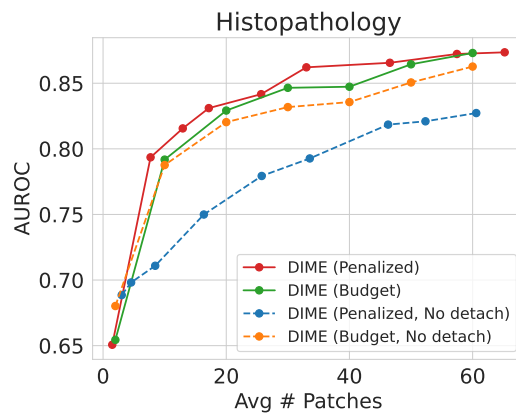


Figure 14: Ablation of stop-gradients trick when using prior information for the histopathology dataset (Appendix C).

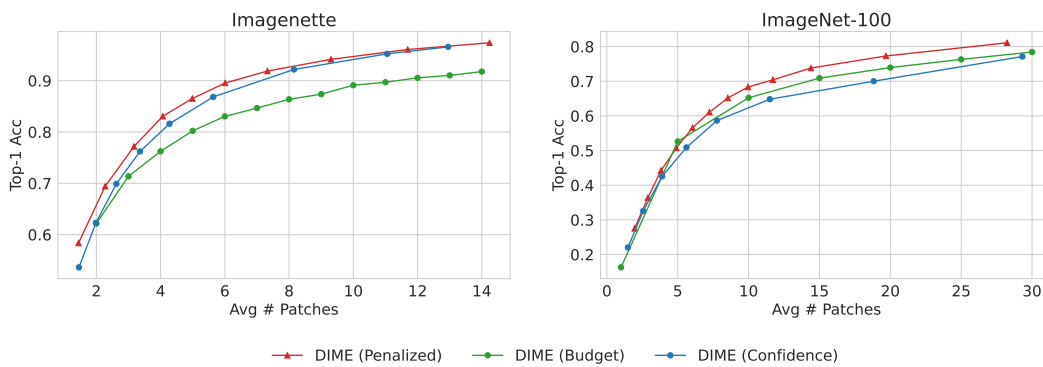


Figure 15: Comparison of the budget-constrained and penalized stopping criteria with the confidence-constrained approach.